NAVAL POSTGRADUATE SCHOOL

MONTEREY, CALIFORNIA

THESIS

TERMINAL HOMING POSITION ESTIMATION FOR AUTONOMOUS UNDERWATER VEHICLE DOCKING

by

Mkuseli Mqana

June 2017

Thesis Advisor:	Douglas Horner
Second Reader:	Sean Kragelund

THIS PAGE INTENTIONALLY LEFT BLANK

REPORT DOCUMENTATION PAGE			*Form Approved OMB No. 0704–0188*

1. AGENCY USE ONLY *(Leave blank)*	**2. REPORT DATE** June 2017	**3. REPORT TYPE AND DATES COVERED** Master's thesis

4. TITLE AND SUBTITLE TERMINAL HOMING POSITION ESTIMATION FOR AUTONOMOUS UNDERWATER VEHICLE DOCKING	**5. FUNDING NUMBERS**
6. AUTHOR(S) Mkuseli Mqana	
7. PERFORMING ORGANIZATION NAME(S) AND ADDRESS(ES) Naval Postgraduate School Monterey, CA 93943-5000	**8. PERFORMING ORGANIZATION REPORT NUMBER**
9. SPONSORING /MONITORING AGENCY NAME(S) AND ADDRESS(ES) N/A	**10. SPONSORING / MONITORING AGENCY REPORT NUMBER**

11. SUPPLEMENTARY NOTES The views expressed in this thesis are those of the author and do not reflect the official policy or position of the Department of Defense or the U.S. Government. IRB number ____N/A____.

12a. DISTRIBUTION / AVAILABILITY STATEMENT Approved for public release. Distribution is unlimited.	**12b. DISTRIBUTION CODE**

13. ABSTRACT (maximum 200 words)

This study aims at developing an improved methodology for position estimation by which sparse, erroneous and inconsistent sensor observations can be utilized for Autonomous Underwater Vehicle (AUV) terminal homing to an undersea docking station.

An undersea docking station offers great potential for increasing AUV at-sea time and reducing survey costs. A key part of this system is the ability of the AUV to successfully dock. Part of the process for successful docking is AUV position estimation. The Digital Ultra-Short Baseline (D-USBL) is a sensor system used by the AUV to provide range and bearing measurements to the docking station. These measurements can be used by the AUV to improve its position estimate.

Due to the nonlinearity of the D-USBL measurements, the Extended Kalman Filter (EKF), Unscented Kalman Filter (UKF) and forward and backward smoothing (FBS) filter were utilized to estimate the position of the AUV. After performance of these filters was deemed unsatisfactory, a new smoothing technique called the Moving Horizon Estimation (MHE) with epi-splines was introduced. The MHE smoothing filter used the dead reckoning measurements and the D-USBL measurements as constraints in the epi-splines optimization method.

The analysis based on data sets of REMUS 100 AUV docking station runs was conducted using the MHE/epi-splines methodology and compared to EKF and UKF algorithms. The MHE/epi-splines algorithm demonstrated significantly better performance over the EKF and UKF.

14. SUBJECT TERMS ®Position Estimation, EKF, UKF, FBS, MHE, epi-spline, docking station, technique, USBL, measurements, REMUS, AUV	**15. NUMBER OF PAGES** 97
	16. PRICE CODE

17. SECURITY CLASSIFICATION OF REPORT	**18. SECURITY CLASSIFICATION OF THIS PAGE**	**19. SECURITY CLASSIFICATION OF ABSTRACT**	**20. LIMITATION OF ABSTRACT**
Unclassified	Unclassified	Unclassified	UU

NSN 7540–01-280-5500 Standard Form 298 (Rev. 2–89) Prescribed by ANSI Std. 239–18

THIS PAGE INTENTIONALLY LEFT BLANK

Approved for public release. Distribution is unlimited.

TERMINAL HOMING POSITION ESTIMATION FOR AUTONOMOUS UNDERWATER VEHICLE DOCKING

Mkuseli Mqana, Armament Corporation of South Africa
B. Eng., University of Pretoria, 2007

Submitted in partial fulfillment of the
requirements for the degree of

MASTER OF SCIENCE IN MECHANICAL ENGINEERING

from the

NAVAL POSTGRADUATE SCHOOL
June 2017

Approved by: Douglas Horner, Ph.D.
Thesis Advisor

Sean Kragelund, Ph.D.
Second Reader

Garth Hobson, Ph.D.
Chair, Department of Mechanical and Aerospace Engineering

THIS PAGE INTENTIONALLY LEFT BLANK

ABSTRACT

This study aims at developing an improved methodology for position estimation by which sparse, erroneous and inconsistent sensor observations can be utilized for Autonomous Underwater Vehicle (AUV) terminal homing to an undersea docking station.

An undersea docking station offers great potential for increasing AUV at-sea time and reducing survey costs. A key part of this system is the ability of the AUV to successfully dock. Part of the process for successful docking is AUV position estimation. The Digital Ultra-Short Baseline (D-USBL) is a sensor system used by the AUV to provide range and bearing measurements to the docking station. These measurements can be used by the AUV to improve its position estimate.

Due to the nonlinearity of the D-USBL measurements, the Extended Kalman Filter (EKF), Unscented Kalman Filter (UKF) and forward and backward smoothing (FBS) filter were utilized to estimate the position of the AUV. After performance of these filters was deemed unsatisfactory, a new smoothing technique called the Moving Horizon Estimation (MHE) with epi-splines was introduced. The MHE smoothing filter used the dead reckoning measurements and the D-USBL measurements as constraints in the epi-splines optimization method.

The analysis based on data sets of REMUS 100 AUV docking station runs was conducted using the MHE/epi-splines methodology and compared to EKF and UKF algorithms. The MHE/epi-splines algorithm demonstrated significantly better performance over the EKF and UKF.

THIS PAGE INTENTIONALLY LEFT BLANK

TABLE OF CONTENTS

LIST OF FIGURES

LIST OF TABLES

THIS PAGE INTENTIONALLY LEFT BLANK

LIST OF ACRONYMS AND ABBREVIATIONS

ACDP	Acoustic Doppler Current Profiler
AUV	Autonomous Underwater Vehicle
CAVR	Center for Autonomous Vehicle Research
DC	Direct Current
D-USBL	Digital Ultra-Short Baseline
DVL	Doppler Velocity Log
DVR	Digital Video Recorder
EKF	Extended Kalman Filter
FBS	forward and backward smoothing
GNC	Guidance, Control and Navigation
GPS	Global Positioning System
GRV	Gaussian Random Variables
IMU	Inertial Measurement Unit
INS	Inertial Navigation System
LBL	Long Baseline
MBARI	Monterey Bay Aquarium Research Institute
MHE	Moving Horizon Estimation
NED	North East Down
NPS	Naval Postgraduate School
REMUS	Remote Environmental Monitoring Units
UKF	Unscented Kalman Filter
UT	Unscented Transformation
UTP	Underwater Transponder Positioning
WHOI	Woods Hole Oceanographic Institution

THIS PAGE INTENTIONALLY LEFT BLANK

ACKNOWLEDGMENTS

I thank my sponsor, Armscor, and the managers of the Institute of Maritime Technology, Danie Bence and Chris Kruyshaar, for nominating and encouraging me to pursue my master's in Mechanical Engineering.

I thank my thesis advisor, Professor Douglas Horner, for spending all of his available time showing me everything he could about the REMUS 100 AUV. He made me realize that, with the best guidance, anything is possible. I would also like to thank Dr. Sean Kragelund, my second reader, for all of his work in making sure that we completed this thesis.

I thank my wife, Nosive Lumka Mqana, for her trust and the respect she has for me—even though I was on the other side of the world—and for keeping our family together.

I would also like to thank all my lecturers and classmates for supporting me during my studies at NPS.

THIS PAGE INTENTIONALLY LEFT BLANK

I. INTRODUCTION

A. MOTIVATION

The autonomous underwater vehicle (AUV) has taken center stage in defense underwater surveys. AUVs are capable of doing more work over a short period while maintaining low operational costs. As of 2017, AUVs are used to conduct mine hunting operations, sea floor mapping and other important activities previously conducted by divers. In the civilian environment, AUVs are used mostly to inspect underwater pipes for maintenance purposes. Most civilian companies invest their resources into ensuring they have the best AUV with the latest equipment onboard to achieve their mission requirements successfully. The challenge facing the underwater robotics community is the cost of deploying and extracting these AUVs under potentially bad weather conditions. AUVs have limited operational duration due to their rechargeable battery capacity and their data storage capacity. An undersea docking station offers great potential for increasing at-sea time and reducing survey costs of AUVs. An undersea docking station provides the AUV's battery recharging facility, data download and offload activities. The key part of using the undersea docking station is the ability of the AUV to dock. Once the AUV has docked in an undersea docking station, the batteries will be recharged and the data will be transferred to the user on the surface stations and the vehicle mission will be updated. The use of an undersea docking station permits the AUV to remain at sea for extended periods of time.

B. PROBLEM STATEMENT

The purpose of this study is to develop a methodology for position estimation by which sparse, erroneous, and inconsistent sensor observations can be used for AUV terminal homing to an undersea docking station. An undersea docking station offers great potential for increasing at-sea time and reducing survey costs of AUVs. A key part of this system is the AUV's ability to successfully dock. Part of the process for successful docking is estimating the AUV's position. The AUV's digital ultra-short baseline (D-USBL) sensor system provides range and bearing measurements to the docking station.

The D-USBL range and bearing measurements are nonlinear, sparse, erroneous and inconsistent.

Figure 1, courtesy of Horner and Mqana [1], shows a REMUS 100 AUV with a Woods Hole Oceanographic Institution (WHOI) docking station used by the Naval Postgraduate School (NPS)'s Center for Autonomous Vehicle Research (CAVR). The docking station is mounted on the ocean floor in the vicinity of the Monterey Inner Shelf Observatory in Monterey Bay, California. The image shows the REMUS 100 successfully docked at the docking station. The docking station has a vertical USBL transponder affixed to the top, a big yellow cylindrical tank housing a 9.6 kWh battery pack, and a camera next to the USBL transponder. The vehicle is prohibited from traveling under the docking station by plexiglass, shown as the black object at the bottom of the image [1].

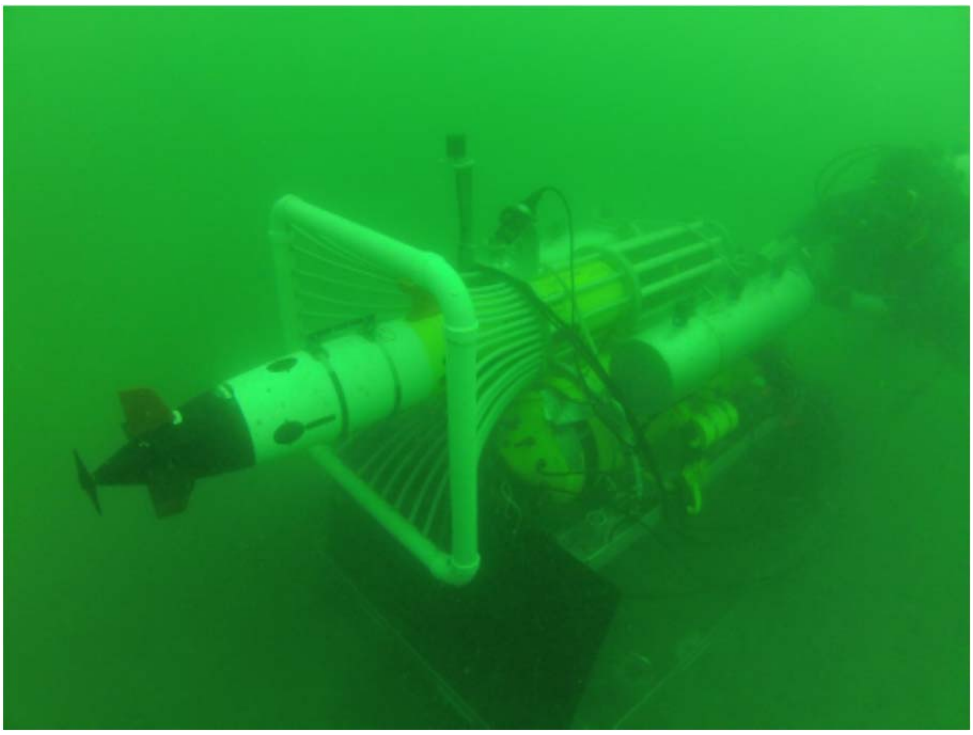

Figure 1. NPS REMUS 100 with WHOI Docking Station. Source: [1].

The AUV starts the terminal homing phase in an undersea docking station operation on the sea surface with access to Global Positioning System (GPS)

measurements. As the vehicle dives deeper underwater, it loses the GPS fixes and relies on the measurements received from dead reckoning sensors such as Doppler Velocity Log (DVL), Inertial Navigation System (INS), Depth sensor and Inertial Measurement Unit (IMU). These sensors have various sampling rates not exceeding 10Hz and the position uncertainty grows linearly over distance travelled. In order to minimize the navigation error as the AUV begins the docking sequence, the AUV is installed with a D-USBL sensor on the bow and the docking station is installed with USBL transponder. The AUV initiates an interrogation of the docking station transponder and it continues to send a periodic sound pulse. When the AUV is within range it may receive a response and transform it to range and bearing. The range and bearing measurements are then used with dead reckoning measurements to update the position of the AUV. The challenge in position estimate for the AUV is how to properly incorporate these infrequent, potentially erroneous and inconsistent measurements into the position estimation filter.

This study aims at developing a methodology that can utilize the sparse, erroneous and inconsistent USBL measurements to guide the AUV to an undersea docking station. The USBL range and bearing measurements are nonlinear in terms of the process used to compute them and in terms of their inconsistency. Due to nonlinearity of the USBL range and bearing measurements, the nonlinear position estimating filters such as Extended Kalman Filter (EKF), Unscented Kalman Filter (UKF) and forward and backward smoothing (FBS) are considered as possible solutions and evaluated using previous REMUS 100 AUV docking station runs. Additionally, a modified, Moving Horizon Estimation (MHE) position estimating method is developed and compared with the alternative methods. The MHE approach is novel due to the use of a non-linear least squares optimization approach known as epi-splines. Results between the methods are compared and contrasted using simulated and in-water results.

C. LITERATURE REVIEW

1. REMUS 100 Vehicles

The REMUS 100 vehicle was first used for coastal monitoring missions, but recently, it has been used in many underwater operations by both defense and civilian

industries [2]. REMUS 100 is an AUV designed to operate within 100 m of the ocean's surface. REMUS 100 is cylindrical in shape and portable in size, so it can be carried by two persons. The modular design of the REMUS 100 ensures relatively easy interchanging of components depending on mission requirements.

Current designs come with the latest technology to maintain high performance and engineering quality. Although the size of the instrumentation has decreased, the vehicle's endurance and performance has increased. REMUS 100 vehicles were originally designed by the Woods Hole Oceanographic Institution (WHOI) lab in the United States. The technology was further developed by Hydroid, Inc. and this company was eventually purchased by Kongsberg Maritime of Norway [3]. These vehicles are attractive to users because they are relatively inexpensive and light-weight as well as easily operated by a trained operator via a standard laptop computer.

2. Underwater Docking Stations

In the past, underwater missions were short and quick. Now, with advanced technology, underwater missions can be as long as the user desires. The new AUVs have better instrumentation, which produces high-quality results, and conduct longer operations. The latest method for ensuring that the underwater environment is well-known by the users is to keep the AUV underwater and ready for the next operation. Underwater docking stations help ensure that the vehicle is kept underwater with charged batteries and with an updated mission plan.

Underwater docking stations are connected to the base station by a communication cable that allows the vehicle to recharge its batteries and transfer data. Underwater docking stations save time for deploying the vehicle and retrieving it after the mission. They also save time transferring data and loading the new mission. The underwater docking stations also help to increase the mission time.

Most underwater docking stations are tapered in shape, or funnel shaped, to catch the cylindrical vehicle when it misses the center of the docking station. The conical shape can complicate the docking event because the AUV can approach the docking station

from only one direction unless the entrance cone pivots around a central axis, B. W. Hobson et al. [4].

B. W. Hobson et al. [4]. at the Monterey Bay Aquarium Research Institute (MBARI) developed and used the underwater docking station for docking the institute's twenty one inch-diameter AUV. MBARI's docking station is shown in Figure 2. This underwater docking station has had many successful docking events, which included transferring data, recharging batteries, and completing the power cycle of the AUV.

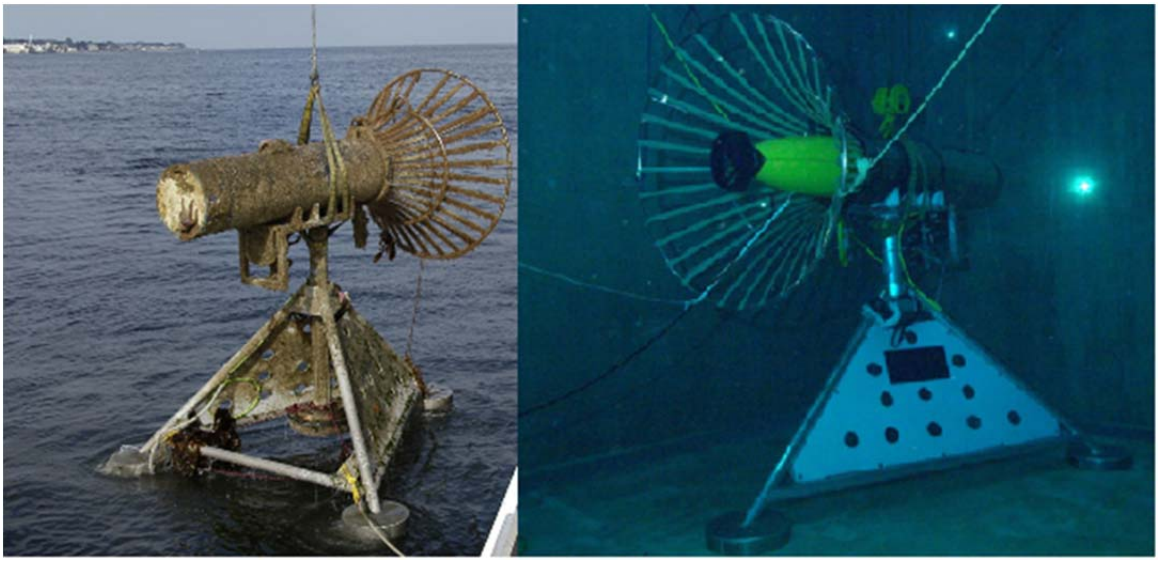

Figure 2. MBARI AUV Docking Station. Source: [4].

Another interesting underwater docking station was designed by C. J. von Alt et al. [5]. The cone section of its underwater docking station is slightly different from the one shown in Figure 2. WHOI's underwater docking station, like MBARI's, can transfer data between the AUV and the home unit as well as recharge the AUV's batteries. Figure 3 shows the WHOI's underwater docking station.

Figure 3. Complete AUV Docking Station. Source: [5].

M. D. Feezer et al. [6]. conducted underwater docking operations using an electromagnetic homing system to estimate the optimal position and orientation of the AUV. M. D. Feezer et al. installed a transmitter on the underwater docking station and a receiver on the AUV. Figure 4 diagrams how the AUV interacts with the underwater docking station when the electromagnetic homing system is used.

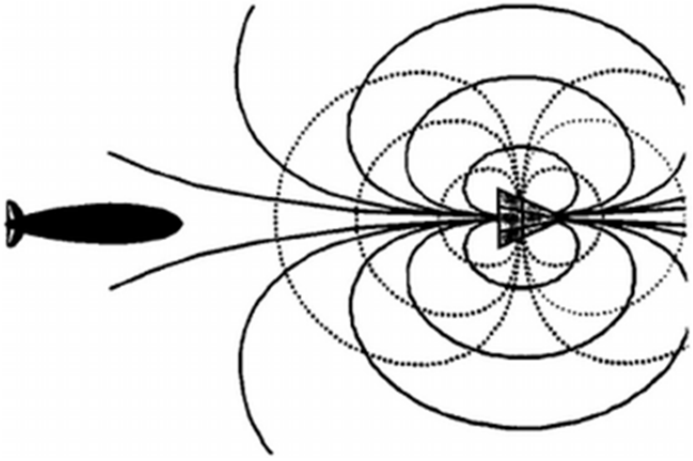

Figure 4. Diagram of an Underwater Docking Station with Electromagnetic Field Lines. Source: [6].

The underwater docking stations with electromagnetic homing have the disadvantage of having to handle unknown interference with nearby metallic objects that produce additional magnetic fields.

Some docking stations are equipped with both optical homing systems and acoustic homing systems to maximize the chances of obtaining a successful docking event. This is a potentially useful approach in that the D-USBL system is used to guide the vehicle from farther away while the camera system can be used to provide final guidance commands. In this study, the underwater docking station is equipped with only a USBL transponder that communicates with the D-USBL sensor installed in the REMUS 100 vehicle.

3. Underwater Docking Environment

As touched upon in the previous section, the undersea environment greatly impacts the sensor performance. Common sensor modalities include vision (optical) homing and acoustics homing methods. The vision homing method is known for its high update-rate advantage. However, the vision (optical) docking method requires relatively clear water visibility. This can be evaluated with the REMUS 100 through the optical backscatter sensor. Baratoff and Blansteen [7] found that the vision homing method can also be degraded by ambient light and infrared radiation. The vision homing method is only effective when the AUV is relatively close to the underwater docking station. Depending on water clarity it is limited to tens of meters.

Figure 5 indicates the possible environment during underwater docking missions. The sea growth can obstruct the view of the AUV when docking using the optical homing method.

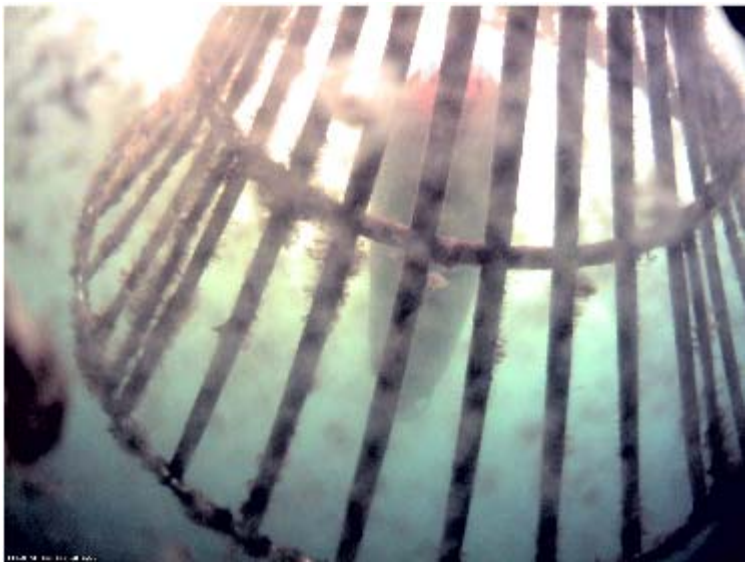

Figure 5. AUV Approaching the Underwater Docking Station. Source: [7].

If the acoustic homing method is used, the sea water needs to be quiet to allow for clear sound propagation between the transponder mounted in the docking station and the D-USBL in the AUV. While visibility does not negatively affect the acoustics homing method, proximity to the sea floor or subsea structures does. Although the acoustic homing method is affordable, it is known for low update rates. Figure 6 shows the MBARI underwater docking station which used an acoustic homing method to dock the twenty one inch Dorado AUV.

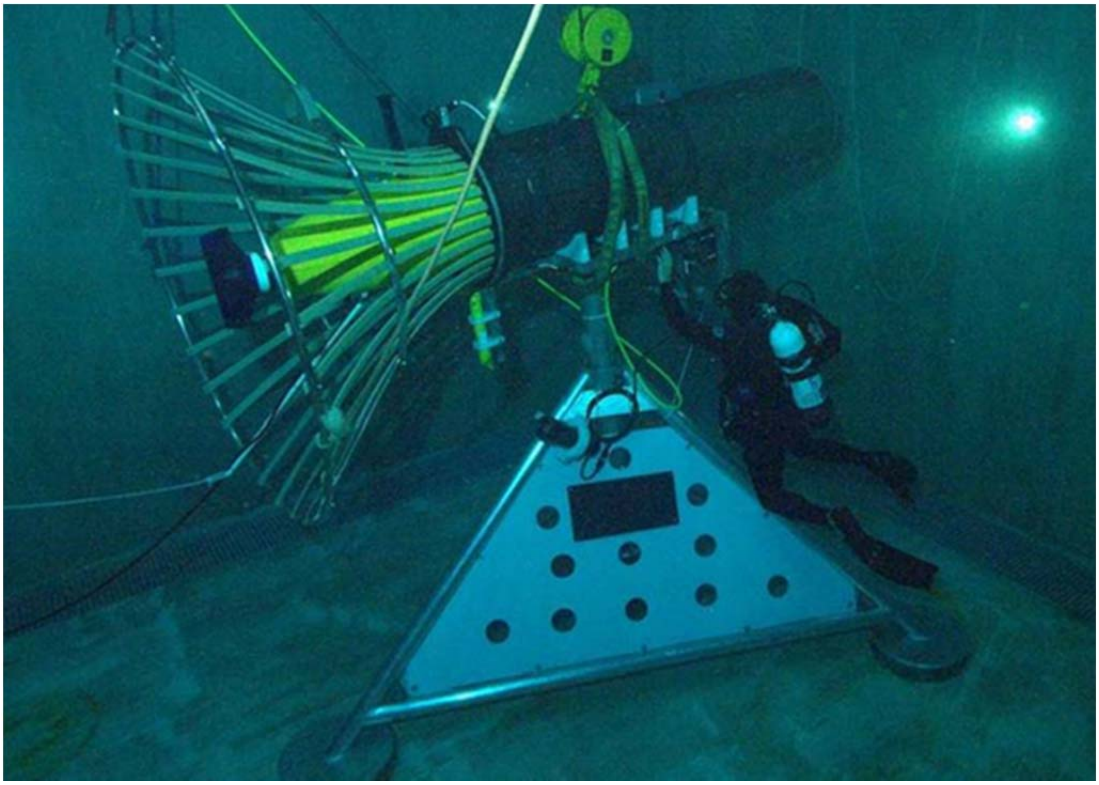

Figure 6. MBARI Underwater Docking Station in Use. Source: [5].

In some cases, the vision and acoustic guidance methods are combined to improve the docking operation. The position of the docking station for this combination should be optimized to ensure that both methods produce usable results, A. Myagotin et al. [8].

4. EKF and UKF Position Estimating Methods

This study evaluates the position estimating methods on using the nonlinear, sparse, erroneous and inconsistent USBL measurements to guide the AUV to an undersea docking station. Some studies are particularly relevant to this thesis. For instance, a few publications have covered the case of tracking underwater vehicles using D-USBL measurements and the optical guidance method. Filip Mandić et al. [9]. used D-USBL and sonar image measurements to track the underwater target precisely. Figure 7 depicts a small grayscale image captured by the forward looking sonar system. D-USBL measurements assist in bounding the uncertainties of the image to identify the object.

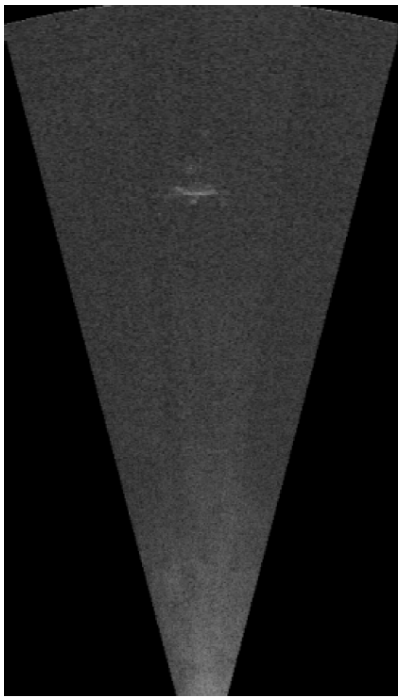

Figure 7. D-USBL and Sonar Image Positioning System. Source: [9].

The EKF was used to estimate the optimal position of the target from the availability of the target image in the sonar's field of view. This study was conducted in two scenarios, one with a moving vehicle and slowly drifting target and one with a static vehicle and moving target. The results were as follows: the position estimate drifted every time the target was outside the sonar's field of view and D-USBL measurements were unavailable. The fusion of the two sensors produced the most accurate tracking results in both scenarios.

D-USBL measurements have become the common method for tracking the position of targets under water. N. Stilinović et al. [10] conducted a study whereby the D-USBL was used to track a diver under water. An AUV that floated on the surface provided the diver below with correct GPS coordinates. N. Stilinović et al. investigated "the guidance and control algorithms for the autonomous surface platform which enables diver tracking" [10]. In the study, the D-USBL was used to track the vertical position of the diver while the GPS was used for horizontal positioning. The EKF was used to provide the diver position estimates. The simulation yielded acceptable results except for

when the diver turned faster than the surface platform, thereby causing errors at the corners.

Unlike the study conducted by Mandić et al. [9]., N. Stilinović et al. [10] tracked the underwater moving object with D-USBL measurements only. The study by Mandić et al. [9]. is closer to the current study because measurements from two sources, sonar imaging and D-USBL measurements, were fused to obtain the optimal state of the underwater object. This thesis intends to apply a fusion of measurements from many AUV built-in sensors such as the DVL, depth sensor, INS, IMU and GPS as well as the D-USBL. The advantage of the current study is that the target is stationary and its position is known.

Ø. Hegrenaes et al. [11] discovered another method of improving underwater navigation and control. Hegrenaes et al. discovered the method called underwater transponder positioning (UTP). This method integrates the AUV's INS with the range measurements from the transponder. The UTP method is similar to the D-USBL but experiences better accuracy due to its tight integration with the INS. Hegrenaes et al. used the Kalman filter to estimate the optimal position of the transponders for this method. Hegrenaes et al. discovered that the UTP aiding method is possible and accurate for large-scale underwater operations [11]. Hegrenaes et al. study is related to this thesis because it used UTP-aided INS sensor measurements to bound the measurement errors. This thesis intends to bound the built-in sensor measurement errors using D-USBL fixes when they are available.

Paul Frontera [12] conducted a study to estimate the state of the system with infrequently available measurement information. Frontera's study aimed at estimating the submarine position without accessing the information from landmarks. Frontera focused on comparing the EKF's and UKF's performances in handling the nonlinear and sparse D-USBL measurements. Frontera discovered that the EKF and UKF show similar performances at short measurement intervals, but the UKF performs better at longer measurement intervals. These findings were expected as the UKF is adept at handling highly nonlinear measurements while the EKF uses second-order Taylor series

approximation, which fails at highly nonlinear measurements. This thesis intends to explore, through simulation, the EKF and UKF optimal state estimation methods.

Another interesting use of the position estimating method appears in a study by Mohammed and Alzubaidi [13]. Mohammed and Alzubaidi used the position estimating method to track an attacking missile and prevent it from hitting its target using the EKF. Mohammed and Alzubaidi found that the estimated positions of the target were more accurate when the target was closer to the object.

The position estimation method is also used in missile guided systems, as described in M. S. Bezick et al. [14]. Bezick et al. explored the "inertial navigation for guided missile using the position, velocity and altitude for missile guidance and control and the inflight alignment technique that can be used to increase the accuracy of the missile navigation system data by incorporating the external non-inertial navigation-aiding data using the Kalman filter and the measurements from the external radar track of the missile and the GPS receiver" [14].

Feezer et al. [6]. used the electromagnetic homing system to bound the errors produced by the AUV's dead reckoning systems when performing the underwater docking operation. The electromagnetic homing method provides the AUV's bearing and orientation, which are very important for successfully docking, especially when the AUV is close to the docking station. The electromagnetic homing system was found very effective at a range of 25 m to 30 m from the docking station. This method can also be used for multiple targets tracking at the same time. The tracking method in [6] works similar to the optical homing method explored by Mandić et al. [9]. Both methods provide good update rates but only at closer ranges.

N. Nadarajah et al. [15] conducted a study to improve "the estimates for a multi target tracking problem using fixed-lag smoothing" [15]. Nadarajah et al. performed the fixed-lag tracking using forward filtering followed by backward smoothing. The standard Kalman filter performed forward filtering in fixed-lag smoothing while the information filter performed backward smoothing. Although these filters use different sets of

measurements, they should converge into one optimal estimate. Such a method is explored in this thesis and may be integrated into the final guidance algorithm.

The EKF was also used to estimate the optimal position and attitude of spacecraft flying in formation. This study was conducted by S. Kim et al. [16]. Given the study's success in tracking moving and stationery targets using position estimating methods, it is highly possible to guide an AUV to a stationary underwater docking station using no GPS measurements and relying solely on sparse D-USBL fixes to bound the state estimation errors.

5. Moving Horizon Estimation Position Estimating Method

Moving horizon estimation (MHE) is the estimation method that considers the constraints of vehicle dynamics while maintaining a minimum error between the estimate and actual data. Although the MHE originated in the 1960s, it is now regarded as an important technique for position estimation for dealing with nonlinear data sampled at multisampling rates with outliers. The MHE has been applied in many different estimation scenarios by Royset and Wets [17].

The advantage of the MHE over the other estimation techniques is that it uses constraints to ensure the estimation results are not influenced by outlier measurements. This property forces the user to establish constraints from the beginning of MHE usage. M. W. Mehrez et al. [18] used the MHE to estimate the position of multiple robots when the initial estimate was unknown. Mehrez et al. chose the MHE over the well-known EKF due to its advantage of working without knowing the initial estimate. The MHE performs a high number of iterations and converges more quickly to the solution with the accepted error range. The EKF is highly affected by the initial conditions and may diverge. The study by Mehrez et al. found the MHE is unaffected by any kind of distribution. The challenge for the MHE, however, is solving linear programming at every time step. In Mehrez et al's the study, the MHE performed better when the initial position estimate of the robot was unknown. The MHE uses the least squares approximation to overcome the nonlinearity of the measurements and to obtain prior knowledge to generate effective estimates when none are available.

The level of errors and rate of convergence produced by the MHE makes it attractive to the environment of noisy sensors and limited measurements in multi-rate systems. Andong and Wen-An [19] defines the MHE as "an optimization approach that produces estimates of states by using moving limited observed information." Andong and Wen-An investigated the estimation performance of the MHE on a system that produces measurements at different sampling rates. The study employed an inertial sensor and camera to locate the position of a mobile robot. The MHE was used to merge the information from these two sources to improve the estimation results.

The goal of the MHE is to minimize the objective function. The objective function comprises two parameters, the arrival cost and the stage cost. M. K. Ramalingam [20] defines the arrival cost as the uncertainty in the a priori estimate. Approximating the arrival cost is the main challenge for the MHE. The arrival cost is computed using nonlinear filters and passed to the MHE for optimization. If the nonlinear filter, such as the UKF, produces a poor estimate of the arrival cost, the MHE's initial optimization will also be poor. M. A. Müller [21] introduced the MHE scheme that confirms the assumption of prior weighting in the cost function offline.

The MHE can be applied in many estimation environments. M. Zanon et al. [22] used the nonlinear version of the MHE to find estimates for the friction coefficient of autonomous vehicles travelling on the road. Zanon et al. used the direct multiple shooting method to find the estimated friction coefficient between the tires and the road. The study used least squares nonlinear programming as a mathematical tool to execute the computations in the MHE application. Zanon et al. also used the real-time iteration scheme with shifting since the computational effort for optimization is high for real-time feedback control purposes.

According to Zanon et al. [22], "The real time iteration is also found to reduce the latency between the instant when the measurements are available and the instant when the feedback is available by preparing the computations as much as possible even before the measurements are available." The MHE produced estimates for the friction coefficient in the study within milliseconds at the complexity of highly nonlinear models.

The MHE is sometimes used with epi-splines as a nonlinear least-squares cost-function minimization technique.

Epi-splines were also used by Royset and Wets [17] in the article entitled "From Data to Assessments and Decisions: Epi-Spline Technology." Royset and Wets defines epi-splines as "the newly developed piecewise polynomial functions described by the finite number of parameters, which are exceptionally flexible." As described in the article, epi-splines are used for image reconstruction, the probability density estimation of simulation output, as well as electricity demand forecasts with respect to weather conditions. In all of these applications, epi-splines were highly effective at predicting results. The effectiveness of the MHE depends on the mode of the probability density function [17].

6. Forward and Backward Smoothing Position Estimating Method

The forward and backward smoothing is a technique applied to the measurements to obtain an optimal smoothed estimate, as described in D.J. Simon [23]. This technique results in two optimal estimates. The first estimate is obtained using an ordinary Kalman filter running forward in time from the first USBL measurement to the USBL measurement at the median of the measurements interval. The second estimate is obtained using an information filter running backward in time from the last measurement in the interval to the measurement at the median of the measurements interval. D.J. Simon [23] states that two estimates are unbiased because they are the outputs of the filters. The two estimates are combined according to their Kalman gains.

The covariance of the forward smoothing step is initiated as a big finite value while the covariance for the backward smoothing step is infinite [23]. Since the infinite is not a valid number for computational purposes, the information filter is used for the inverse of the infinite covariance. The information filter uses zero as the confidence at its starting point. A zero confidence for the information filter means there is no knowledge of the state at the starting point. For computational purposes, the certainty of the information filter is initiated at small numbers greater than zero [23].

The knowledge of the state at the information filter initialization point is key for better performance of backward smoothing. Simon states that if the position of the object is unknown at the information filter starting point, the state's initial condition should be zero, and the state will be updated only by observation and the Kalman gain. This could cause the information filter to diverge if the actual state is far away from the information filter starting position.

D. STRUCTURE OF THE THESIS

This thesis is divided into seven chapters. Chapter II provides an overview of the systems used in this thesis. Chapter III contains the problem description and simulated analysis of the UKF and EKF position estimating techniques. Chapter IV contains the detailed description of the Moving Horizon Estimation (MHE) with epi-spline algorithm. Chapter V presents the results from using UKF, EKF and MHE on previous REMUS 100 docking station runs. Chapter VI contains a detailed description of the FBS position estimating method as well as analysis results whereby the FBS is evaluated and compared to the UKF, EKF and MHE position estimating techniques. Chapter VII concludes the paper.

II. SYSTEM OVERVIEW

A. NPS REMUS 100 VEHICLE DESCRIPTION

The NPS REMUS 100 vehicle has an aft propeller with two aft through-body thrusters (vertical and horizontal) and two forward through-body thrusters (vertical and horizontal). The NPS REMUS 100 vehicle was designed and manufactured by Hydroid and can operate to a maximum depth of 100 m. REMUS 100 vehicles are equipped with propellers and fins for moving forward and for diving. The main navigational sensors installed in the NPS REMUS 100 vehicles includes a GPS unit, Doppler Velocity Log (DVL), Acoustic Doppler Current Profiler (ADCP), depth sensor, Inertial Navigation System (INS), Inertial Measurement Unit (IMU) and other instruments as required by the user. One of the NPS REMUS 100 AUVs at the Center for Autonomous Vehicle Research is shown in Figure 8. This AUV is installed with standard REMUS 100 sensors to execute the underwater docking mission. The color segments indicate the modules used to make this AUV.

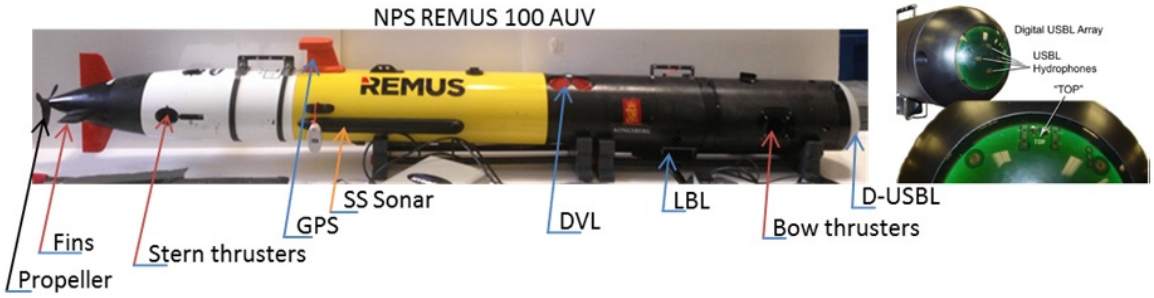

Figure 8. One of the NPS REMUS 100 AUV

When the vehicle is in water, it can use acoustic navigation to conduct an undersea survey in a given area. When the AUV gets underway, the sensors onboard start sampling and recording the data as the vehicle proceeds through the navigation objectives. The REMUS 100 has a control computer that guides the vehicle's operation. REMUS 100 vehicles could replace divers in dangerous underwater operations. With the battery recharging and mission data-transfer capabilities of the underwater docking

stations, the REMUS 100 vehicles could spend more time and collect more meaningful data underwater at lower operating costs. Table 1 lists the physical specifications of the NPS REMUS 100 vehicle.

Table 1. NPS REMUS 100 Vehicle Specifications. Source: [24].

Platform	REMUS 100
Body Type	Torpedo
Body Size (L x W x H)	2.22 m x 0.19 m x 0.19 m
Hull Material	Aluminum
Weight	52 kg to 64.5 kg in air
Operational Depth	3 m to 100 m
Typical Search Area	1200 m x 1000 m
Dynamic Buoyancy	No
Self-Righting	Yes
Obstacle Avoidance	No
Endurance (Nominal Load)	22 hrs at 1.5 m/s and 8 hrs at 2.6 m/s
Propulsion System	Thrusters with direct drive DC brushless motors
Degrees of Freedom	3 degrees of freedom controlled by fins
Nominal Speed	1.54 m/s
Maximum Forward Speed	2.6 m/s

The NPS REMUS 100 AUV is equipped with the built-in sensors and the modular sensors listed in Table 2.

Table 2. NPS REMUS 100 Onboard Sensors

Vehicle built-in sensors	• GPS • Long baseline (LBL) • Acoustic Modem • Kearfott INS • Side Scan Sonar • Acoustic Doppler Current Profiler (ACDP)/Doppler Velocity Log (DVL) • Conductivity Temperature Depth sensor • Optical Backscatter
Vehicle modular sensors	• Blueview Forward and Downward looking sonar • Downward looking Digital Video Recorder (DVR) • Digital Ultra Short Baseline (D-USBL)

Eric B. Bermudez [24] gives a full description of the NPS REMUS 100 vehicle equipment. The key component is the USBL hydrophone on the bow of the vehicle and the acoustic modem (located underneath just forward of the DVL). The D-USBL is an acoustic navigational aid for the REMUS vehicle, according to the REMUS/Swordfish Operations & Maintenance Manual [25]. The D-USBL consists of a potted assembly containing a four-channel planar hydrophone array with integral receiver/processor circuit board. The REMUS vehicle uses D-USBL navigation during "transponder home" objectives, when it is closer to the transponder baseline, and sometimes when only one transponder is audible [3].

According to [3], during the D-USBL navigation, the acoustic modem transducer sends interrogation pings at three-second intervals. The D-USBL array receives the acoustic reply from any standard REMUS transponder in the field of view. To determine its position during a mission, the vehicle calculates the range and bearing to the transponder by measuring the difference in receive-times at each of the four hydrophones [3]. Figure 9 shows the four-channel planar hydrophone array.

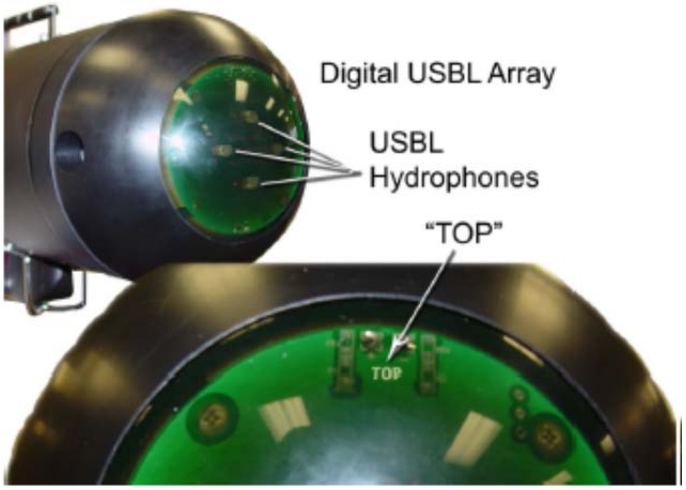

Figure 9. D-USBL Array in Its Nose Cap with Four-Channel Planar Hydrophone Array. Source: [3].

For the vehicle to receive acoustic replies from the transponder mounted on the docking station, the transponder needs to be within +/-35 degrees of the D-USBL's

maximum angle of expected transponder location. Figure 10 illustrates the relative positions of the vehicle and transponder for the best chances of receiving acoustic replies.

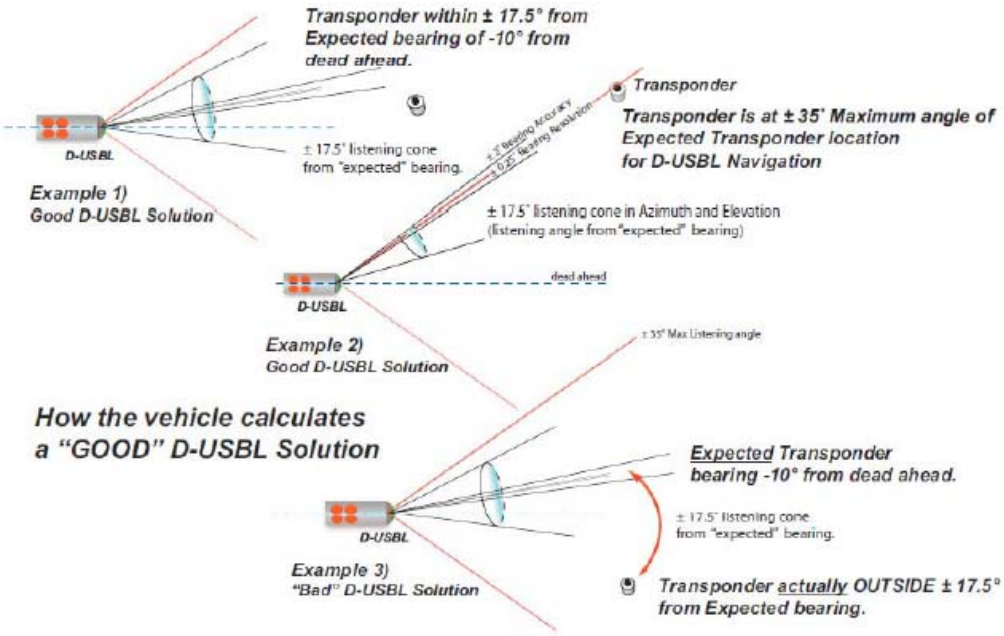

Figure 10. Cone Angle Specifications for D-USBL Measurements. Source: [3].

Table 3 details the performance specifications of the D-USBL from the REMUS/ Swordfish Operations & Maintenance Manual [3].

Table 3. D-USBL Performance Specifications. Source: [3].

Maximum angle from dead ahead	+/- 35 degrees in Azimuth and in elevation
Listening angle	+/- 17.5 degrees in Azimuth and in elevation from the expected transponder bearing
Maximum range	2000 m
Frequency range	20–30 kHz
Bearing accuracy	+/- 2.4 degrees
Bearing resolution	+/- 0.25 degrees
Range (travel time) accuracy	+/- 1ms
Range (travel time) resolution	+/- 80 micro-seconds

The performance specification for the D-USBL is also illustrated in Figure 11.

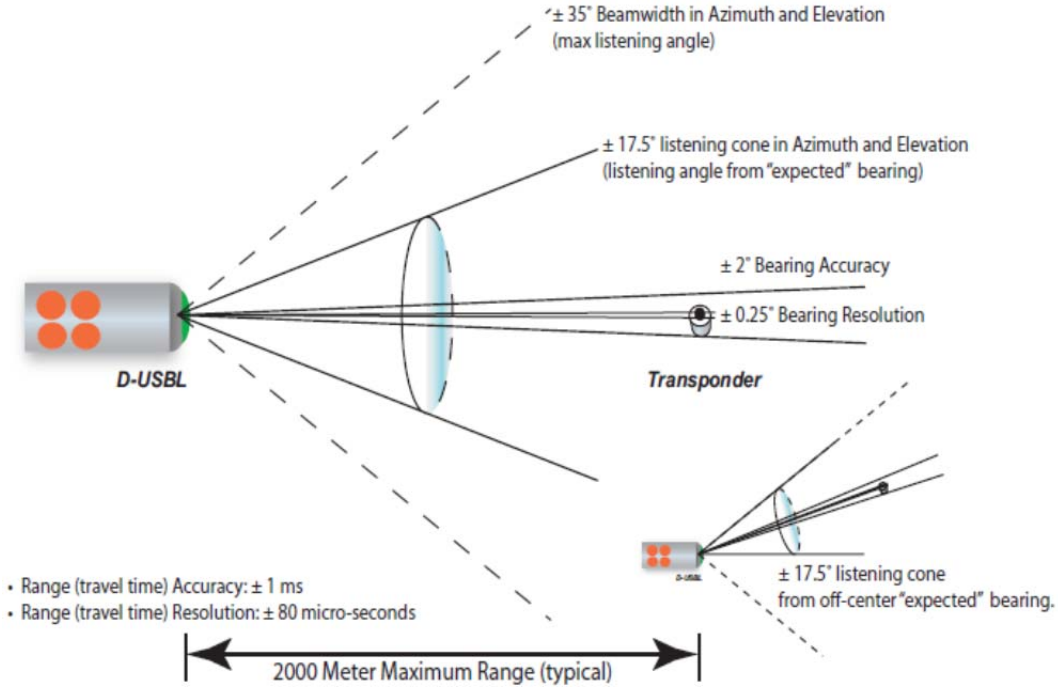

Figure 11. D-USBL Performance Specifications. Source: [3].

B. NPS REMUS 100 DOCKING STATION DESCRIPTION

The purpose of the underwater docking station is to provide a battery recharging facility for the AUV and to serve as an interface for data transfer between the vehicle and the user on shore. The NPS docking station was designed and manufactured by WHOI and supplied to the Center for Autonomous Vehicle Research (CAVR). The docking station came with two ballast tanks that help lower and surface the docking station. The ballast tanks can be filled using a diver's breathing apparatus.

The NPS docking station is powered by a 9.6 kWh battery that is used to recharge the AUV's batteries approximately 10 times and to supply power to other electronic components of the docking station. The NPS docking station is also equipped with a USBL transponder, which is used for terminal homing of the AUV. The docking station has a linear actuator with guide pins that help align the AUV after a successful docking

operation to successfully recharge the batteries and connect to the Ethernet cable for data transfer between the dock and the vehicle.

The entrance to the docking station has a square-shaped opening of 0.7 m by 0.7 m at the larger end of the funnel-shaped entrance. The smaller end of the funnel is circular with a diameter of 0.22 m and becomes the entrance for the cylindrical portion of the AUV when it is successfully docked. The length of the cylindrical opening is 0.93 m.

The D-USBL transponder is mounted 0.42 m above and 0.15 m to the left of the cylindrical centerline, 0.56 m behind the square-shaped end of the funnel. The NPS docking station is also mounted with an underwater camera that helps the user to view and make necessary adjustments to the docking operation. The camera is cable-connected to the dock, which can be connected to a gateway buoy for wireless communication with users at the surface. Figure 12 shows the WHOI docking station which is utilized by the NPS CAVR in the vicinity of the Monterey Inner Shelf Observatory in Monterey Bay, California for undersea docking experiments.

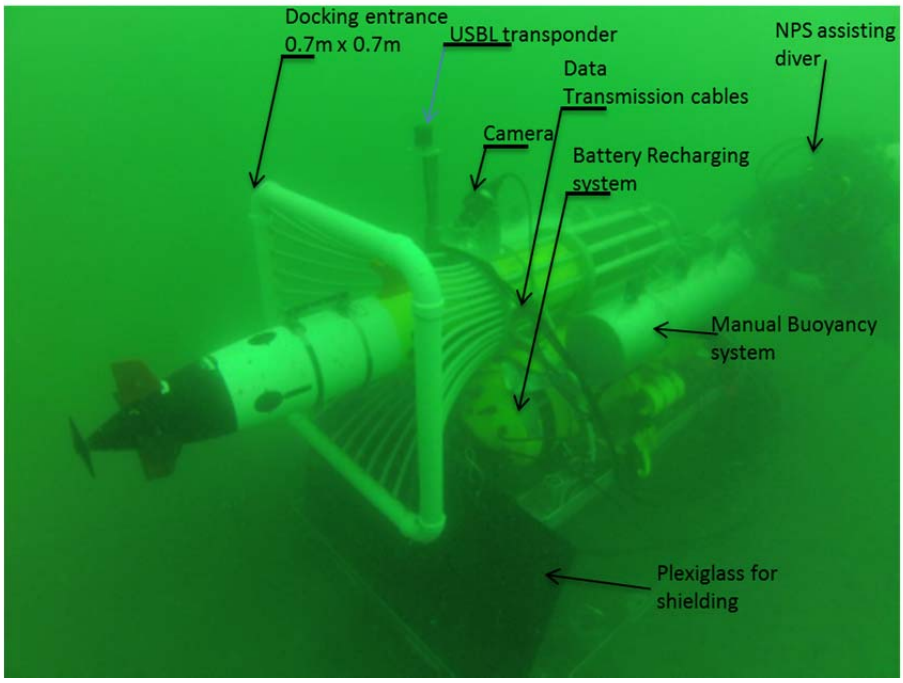

Figure 12. WHOI Docking Station used by NPS CAVR in Monterey Bay, California. Source: [1].

III. PROBLEM DESCRIPTION AND ANALYSIS

The purpose of this study is to develop a methodology for position estimation by which sparse, erroneous, and inconsistent sensor observations can be used for AUV terminal homing to an undersea docking station. An undersea docking station offers great potential for increasing at-sea time and reducing survey costs of AUVs. A key part of this system is the AUV's ability to successfully dock. This is a terminal homing problem where a robust solution addresses Guidance, Control and Navigation (GNC). Guidance is defined as the process of directing the AUV to a desired path or position. Control is defined as the process of maintaining the desired path or position using the feedback controller and considering the external factors. Navigation is defined as the process of localizing the vehicle's position by using position estimation methods. Part of the process for successful docking is estimating the AUV's position. The AUV's D-USBL sensor system provides range and bearing measurements to the docking station. The D-USBL range and bearing measurements are nonlinear, sparse, erroneous and inconsistent.

A. PROBLEM DESCRIPTION

For the purposes of this thesis, the REMUS AUV will use a north-east-down (NED) coordinate system. Using a local reference frame, we define the following variables: longitudinal position (x), lateral position (y), downward position (z), surge velocity (u), sway velocity (v), heave velocity (w), roll angle (Φ), pitch angle (Θ), yaw angle (ψ), as described in T. I. Fossen [25]. These parameters are shown in Figure 13 at their corresponding axis of the AUV. The Inertial reference frame is illustrated by the capital letters X, Y and Z in North, East and Down directions, respectively. The down direction is illustrated by the broken lines in both Inertial and Local reference frames. The Local reference frame is illustrated by the small letter x, y and z directions which are on the body of the vehicle. The vehicle will also be controlled by the yaw-rate (r).

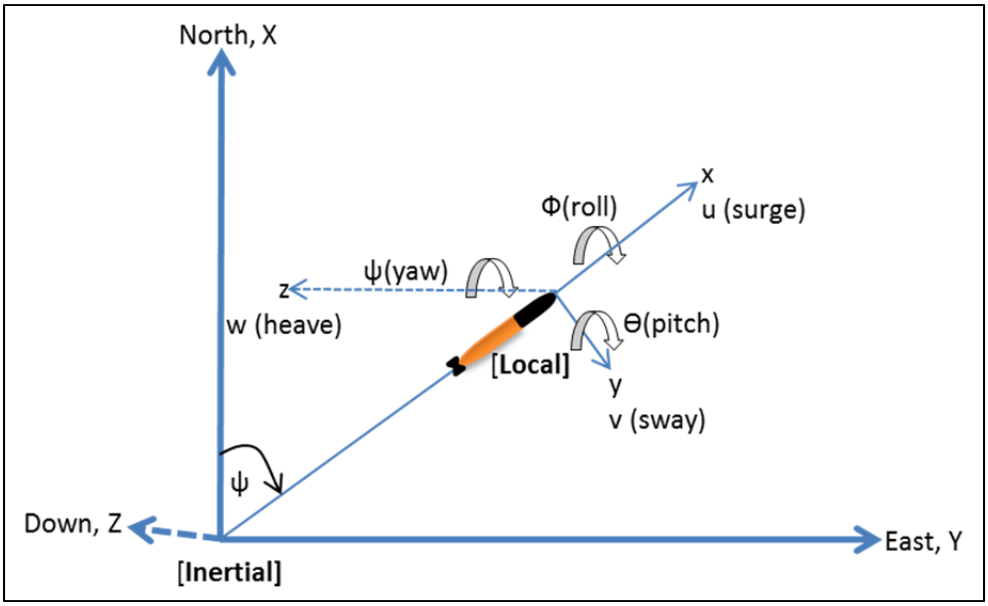

Figure 13. REMUS 100 AUV Axis and Control Parameters. Source: [25].

In this study, the simulated vehicle is an AUV following a set of waypoints and controlled by a cross-track-error controller. The AUV is released at a starting position closer to the first waypoint. The cross-track-error controller always attempts to keep the AUV on its intended track although the dead reckoning instruments cause it to deviate from the track as navigational errors increase with distance traveled.

Figure 14 depicts the underwater setup as explained in this section. The vehicle is shown just past the first waypoint and approaching the second. The AUV track is shown as a red broken line while the intended track is shown as a black broken line.

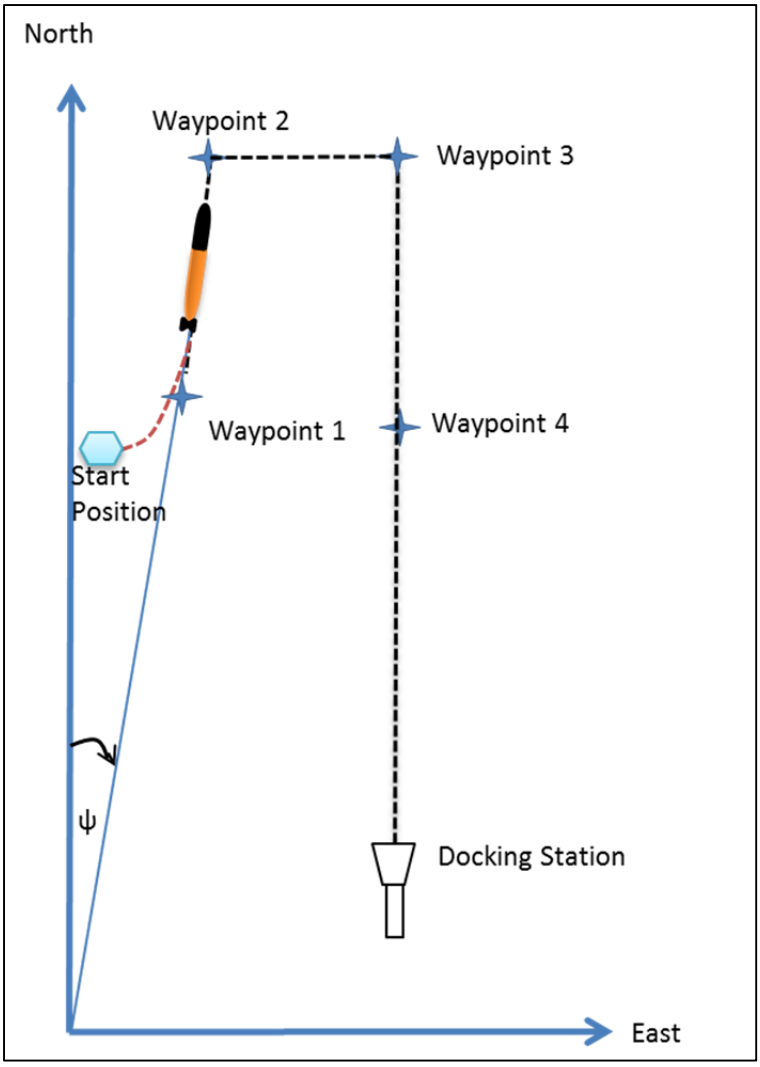

Figure 14. AUV Docking Simulation Setup from Surface to Underwater Docking Station

As the AUV follows the waypoints, the AUV can receive measurements at up to 300m away from the USBL transponder mounted on the docking station. The USBL measurements received by the AUV are arbitrarily distributed and typically non-Gaussian. This makes it difficult to choose a position estimating technique that produces an accurate position estimate for the AUV. Wan and van der Merve [26] describes how the EKF assumes a Gaussian random variable (GRV) distributed state with a mean and variance and performs position estimation, which is accurate up to first-order Taylor series expansion. Given that the EKF can produce huge errors on highly nonlinear

systems, the UKF is also explored in this thesis. The UKF also assumes the state is a GRV distribution, but the UKF uses carefully chosen sigma points to represent the actual state distribution and produces an error of at least second-order accuracy [26]. This terminal homing problem is nonlinear due to the fact that the state propagation equations (the system model) and the range and bearing measurements (the measurement model) are both nonlinear.

Figure 15 shows how the EKF and UKF represent the state distribution. In this figure, the actual state is shown on the left with mean and covariance. The linearized EKF is shown in the middle with Gaussian approximation of the state while the unscented transform (UT), a UKF component, is shown on the right with five carefully placed sigma points to represent the actual state distribution. The true mean, as indicated by a small black circle, is shown at the bottom of each of these representations. As expected, the UKF locates its mean very close to the actual mean with a small variance. Meanwhile, the EKF mean and covariance (shown in red) differ noticeably from the actual mean and covariance (shown in black).

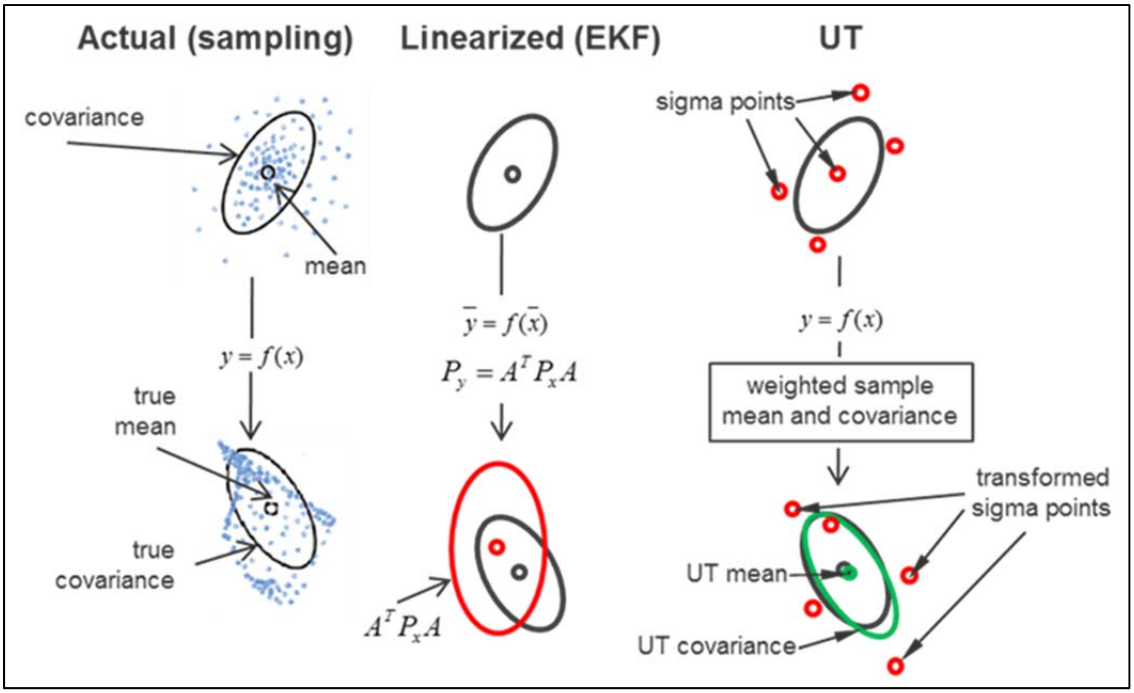

Figure 15. State Distribution as Represented by EKF and UKF (UT). Source: [27].

To further describe the challenge of selecting the best position estimation technique, Figure 16 depicts a high-level view of the AUV docking situation and the way the EKF and UKF represent the measurements. As shown, the UKF distribution can account for many USBL measurements due to the flexibility of placing the sigma points. The EKF is limited to the GRV distribution assumption and can only accommodate few measurements in its distribution. This causes the EKF to be less accurate on highly nonlinear measurements. In this figure, the AUV is shown approaching the region with a high concentration of USBL measurements. The AUV cannot use all measurements due to its dynamic limitations. The position estimation technique should, therefore, produce an optimal mean for the AUV to move in the right direction.

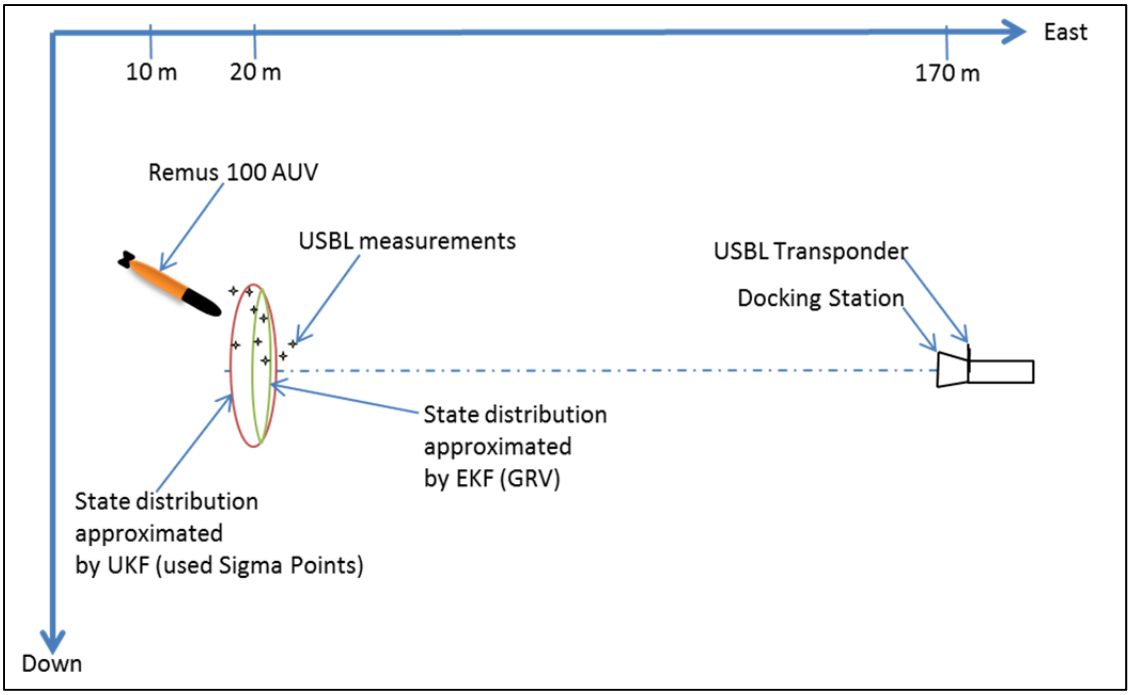

Figure 16. REMUS 100 AUV Docking Scenario and State Representation by UKF and EKF

A general filtering approach is summarized in the flow chart provided in Figure 17. The flow chart shows the measurement model on the left with the measured state. The measurements produced by the built-in AUV sensors such as GPS, INS and DVL are integrated into a single source of measurements with an update rate of not more than 10 Hz. These measurements are then combined with the sparse, inconsistent and erroneous D-USBL measurements with update rate of about 0.2Hz to 1Hz. These measurements are combined in a data fusion process, which comprises the position estimation methods listed. The system model also provides the estimated state to the data fusion block, which fuses all measurements using the EKF or UKF with Kalman gain or by using the MHE with epi-splines. The data fusion results in the optimal estimated state, as illustrated on the right-end of the flow diagram. The optimal estimated state is then fed back to the system model as a new predicted state of the AUV in the next time step. If D-USBL measurements are not available, the vehicle uses the integrated system measurements to dead reckon to its future position.

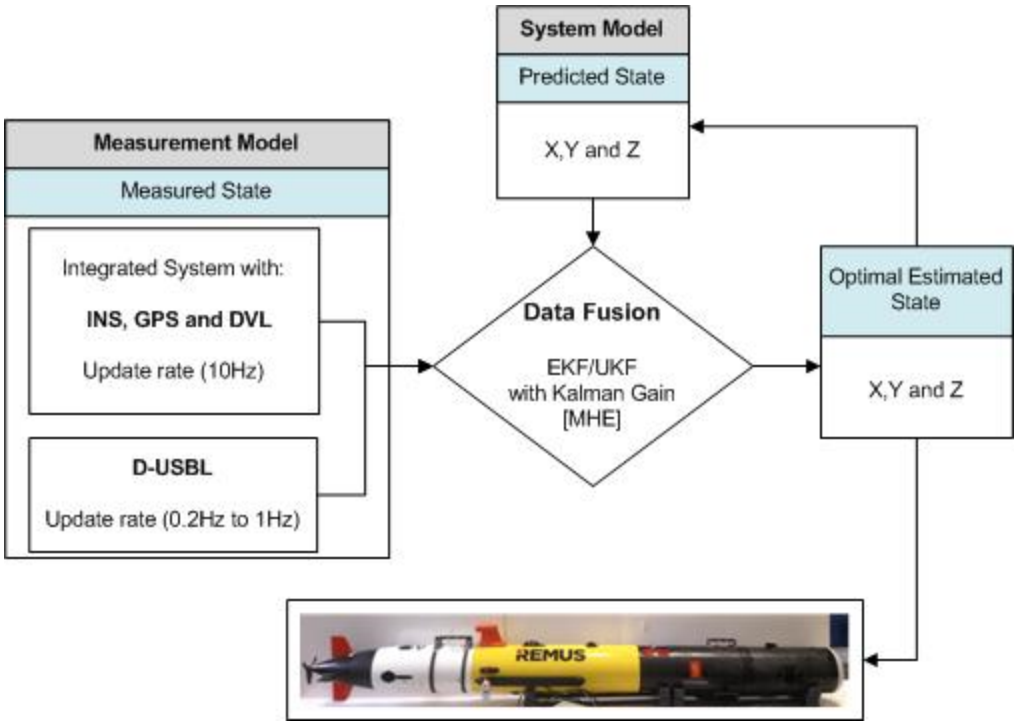

Figure 17. General Data Filtering/Fusion Flow Chart

B. DESCRIPTION OF OPTIMAL ESTIMATION USING EKF

Rhudy and Gu [28] describe the EKF as an important technique in optimally estimating the state of engineering systems using an optimal observer gain to minimize the expected mean squared error of the estimate. The EKF assumes the linear Gaussian nature of the posterior state with mean and covariance to obtain an optimal solution. The EKF approaches the nonlinearity of the system by applying the analytical linearization, which involves using Jacobian matrices. The calculation of the Jacobian is a straightforward operation, but it has the potential for errors.

The EKF is more effective in nonlinear systems up to the second degree of nonlinearity. The EKF becomes less efficient as the degree of nonlinearity increases. Even though the EKF is unlikely to be used on systems with higher levels of nonlinearity, it is simpler to apply and understand than the filters used for highly nonlinear systems.

The main drawback for the EKF is that because solutions are restricted by the Gaussian assumption, highly nonlinear effects of the system are not included in the

variance estimate. This causes the EKF to perform poorly on highly nonlinear systems. According to Einicke and White [29], the EKF linearizes the nonlinear measurement model for its current state estimate and uses the Kalman filter to propagate the state forward in time.

The EKF uses five equations to obtain the optimal solution of the state estimation. The equations are as follows:

Prediction Stage:

System Model

$$\hat{x}_{k|k-1} = f(\hat{x}_{k-1}, u_{k-1}) + w_k \qquad w_k = N(0, \sigma) \tag{1}$$

Measurement Model

$$Z_k = h(\hat{x}_{k-1}) + v_k \qquad v_k = N(0, \sigma) \tag{2}$$

Prior/Prediction Covariance Matrix

$$P_{k|k-1} = A_{k-1} P_{k-1|k-1} A_{k-1}^T + Q_{k-1} \tag{3}$$

Kalman Gain:

$$K_k = P_{k|k-1} H_k^T \left(H_k P_{k|k-1} H_k^T + R_k\right)^{-1} \tag{4}$$

Correction Stage:

$$\hat{x}_{k|k} = \hat{x}_{k|k-1} + K_k\left(Z_k - H_k \hat{x}_{k|k-1}\right) \tag{5}$$

$$P_{k|k} = P_{k|k-1}(I - K_k H_k) \tag{6}$$

In (1) $\hat{x}_{k|k-1}$ is the new estimation at time *k* based on prediction obtained from time *k-1*, and u_{k-1} is the input vector at time *k-1* and is ignored for this study. Function *f* is a nonlinear continuous function; therefore, it is differentiable such that A_{k-1} is a Jacobian based on time *k-1* obtained by differentiating the function *f* with respect to the state $\hat{x}_{k|k-1}$ as given by

$$A_{k-1} = \frac{\partial f}{\partial \hat{x}_{k-1}} | \hat{x}_{k-1} \tag{7}$$

In (2) Z_k is the measurement model based on time *k*, h is the nonlinear function relating the current process state $\hat{x}_k$ to the current measurement Z_k, and v_k is the measurement noise. In (3) $P_{k|k-1}$ is the covariance of the predicted state at time *k* based

on the prediction from time *k-1*, and Q_{k-1} is the covariance of the linearized process model.

In (4) K_k is the Kalman filter gain at time *k*, while H_k is the Jacobian obtained by linearizing the measurement function *h* around the current state as given by

$$H_k = \frac{\partial h}{\partial \hat{x}_k} | \hat{x}_{k|k-1} \tag{8}$$

and R_k is the covariance of the linearized measurement model.

In (5) $\hat{x}_{k|k}$ is the estimate of the mean at time *k* based on new measurements at time *k* and $\hat{x}_{k|k-1}$, while $P_{k|k}$ in (6) is the covariance of the current estimate $\hat{x}_{k|k}$.

In this study, the state transition matrix (*A*) is used to relate the state estimate to the new prediction. The equation showing the relationship between the state estimate and the current prediction is given by the commonly used and convenient first-order linear differential equation:

$$\dot{x} = Ax \tag{9}$$

the solution of which is given by

$$\emptyset = e^{Adt} \tag{10}$$

where *dt* is the time increment in seconds. With this relationship, (1) and (2) become

$$\hat{x}_{k|k-1} = \emptyset_k \hat{x}_{k-1} \tag{11}$$

$$P_{k|k-1} = \emptyset_k P_{k-1} \emptyset_k^T + Q_{k-1} \tag{12}$$

The equations of motion of the vehicle underwater in NED coordinates, assuming roll angle is zero, are as follows:

$$x_k = x_{k-1} + ucos(\theta)\, cos(\psi)\, dt - vsin(\psi)dt \tag{13}$$

$$y_k = y_{k-1} + ucos(\theta)\, sin(\psi)\, dt + vcos(\psi)dt \tag{14}$$

$$z_k = z_{k-1} + usin(\theta)dt \tag{15}$$

The state is then given by

$$\frac{dx_k}{dt} = \dot{x}_k = ucos(\theta)\, cos(\psi) - vsin(\psi) \tag{16}$$

$$\frac{dy_k}{dt} = \dot{y}_k = ucos(\theta)\, sin(\psi) + vcos(\psi) \tag{17}$$

$$\frac{dz_k}{dt} = \dot{z}_k = usin(\theta) \tag{18}$$

Therefore, the state transition matrix A is given by

$$A = \begin{bmatrix} 0\ 0\ 0 & (cos(\theta)\cos(\psi)) & -(sin(\psi)) & 0\ 0\ 0\ 0\ 0\ 0 \\ 0\ 0\ 0 & (cos(\theta)\sin(\psi)) & (\cos(\psi))) & 0\ 0\ 0\ 0\ 0\ 0 \\ 0\ 0\ 0 & sin(\theta) & 0 & 0\ 0\ 0\ 0\ 0\ 0 \\ 0\ 0\ 0 & 0 & 0 & 0\ 0\ 0\ 0\ 0\ 0 \\ 0\ 0\ 0 & 0 & 0 & 0\ 0\ 0\ 0\ 0\ 0 \\ 0\ 0\ 0 & 0 & 0 & 0\ 0\ 0\ 0\ 0\ 0 \\ 0\ 0\ 0 & 0 & 0 & 0\ 0\ 0\ 0\ 0\ 0 \\ 0\ 0\ 0 & 0 & 0 & 0\ 0\ 0\ 0\ 0\ 0 \\ 0\ 0\ 0 & 0 & 0 & 0\ 0\ 0\ 0\ 0\ 0 \\ 0\ 0\ 0 & 0 & 0 & 0\ 0\ 0\ 0\ 0\ 0 \\ 0\ 0\ 0 & 0 & 0 & 0\ 0\ 0\ 0\ 0\ 0 \end{bmatrix}$$

And the matrix x is given by

$$x = \begin{bmatrix} x \\ y \\ z \\ u \\ v \\ w \\ \theta \\ \psi \\ r \\ Range \\ Bearing \end{bmatrix}$$

C. DESCRIPTION OF OPTIMAL ESTIMATION USING UKF

The UKF is one of the most popular state estimation techniques used for nonlinear systems. The UKF is from the same family of filtering systems as the EKF. The UKF is an improved method of filtering from the EKF. Since the EKF is known for producing large errors in higher order systems, it is considered a sub-optimal filter. The UKF, on the other hand, is considered an optimal filter.

The UKF employs the UT, which is used in calculating the statistics of a random variable undergoing a nonlinear transformation [26]. The UKF is accurate up to third-

order Gaussian inputs for all nonlinearities and at least second-order for non-Gaussian inputs [26].

The UKF is an extension of the UT. The UKF is easier to apply than the EKF because it does not make any use of the Jacobians, which may be challenging to evaluate and result in approximation errors [26]. The UKF employs deterministically-chosen weighted sample points known as sigma points to compute its version of the Jacobian and Hessian matrices without performing analytical differentiation. These sigma points are chosen to completely capture the true mean and covariance of current state variables. The UKF is accurate up to third-order Taylor series for any nonlinearity unless the prior random variable has a symmetric distribution such as an exponential family of probability density functions [26].

The following is the final algorithm used by the UKF to provide an accurate state estimate and its covariance. The UKF uses sigma points calculated as follows:

$$\lambda = \alpha^2(L + \kappa) - L \tag{19}$$

where λ is the scaling parameter, and α is the spread of the sigma points. The parameter α ranges between 10^{-4} and 1. When α is small, the sigma points get closer to each other, and when α is big, the sigma points scatter. The parameter L is the length of the state vector, while κ is a tertiary scaling parameter, which is equal to zero in most cases. This scaling parameter is used as a tuning "knob" to reduce estimation errors, as shown by Julier and Uhlmann [30]. The weighted vector for the mean (eta with superscript *m* for mean and subscript *0* for initial condition) is given by

$$\eta_o^m = \frac{\lambda}{L + \lambda} \tag{20}$$

The weighted vector for covariance (eta with superscript *c* for covariance and subscript *0* for initial condition) is given by

$$\eta_o^c = \frac{\lambda}{L + \lambda} + 1 - \alpha^2 + \beta \tag{21}$$

In (21) β is known as the secondary scaling parameter with an optimal value of 2 for Gaussian distributions.

$$\eta_i^m = \eta_i^c = \frac{1}{2(L+\lambda)} \; for i = 1, \ldots 2L \; columns \tag{22}$$

$$\eta^m = \eta_o^m + \eta_i^m \tag{23}$$

$$\eta^c = \eta_o^c + \eta_i^c \tag{24}$$

The number of sigma points (n) depends on the length of the state vector, and the relationship is given by

$$n = 2L + 1 \tag{25}$$

The size of the sigma point matrix is given by

$$\chi_{k-1} = \left[\hat{x}_{k-1} \; \hat{x}_{k-1} + \sqrt{L+\lambda}\sqrt{P_{k-1}} \; \hat{x}_{k-1} - \sqrt{L+\lambda}\sqrt{P_{k-1}}\right] \tag{26}$$

In (26) $\hat{x}_{k-1}$ is the prior state estimate and P_{k-1} is its covariance. $\sqrt{P_{k-1}}$ is given by the Cholesky method Chol(P_{k-1}), where P_{k-1} is the lower triangular matrix and k is the time of the computation. The sigma points are propagated through prediction using

$$\chi_{k|k-1}^i = f\left(\chi_{k-1}^i, u_{k-1}\right) \tag{27}$$

In (27) $i = 0,1, \ldots 2L \; columns \; of \; the \; matrix$, and f is the nonlinear function describing the dynamics of the system. u_{k-1} is the vector containing the input parameters of the system.

The mean is then predicted by

$$\hat{x}_{k|k-1} = \sum_{i=0}^{2L} \eta_i^m \chi_{k|k-1}^i \tag{28}$$

In (28) $\eta_i^m$is the weighted vector for the mean.

The covariance of the predicted state is then given by

$$P_{k|k-1} = Q_{k-1} + \sum_{i=0}^{2L} \eta_i^c \left(\chi_{k|k-1}^i - \hat{x}_{k|k-1}\right)\left(\chi_{k|k-1}^i - \hat{x}_{k|k-1}\right)^T \tag{29}$$

In (29) Q_{k-1} is the process error covariance matrix and η_i^c is the weighted vector for the covariance.

The observation transformation is computed by propagating each sigma point through the observation as

$$\psi_{k|k-1}^i = h(\chi_{k|k-1}^i, u_k) \tag{30}$$

where $i = 0,1, \ldots 2L$, and h is a nonlinear observation function consisting of range and bearing nonlinear functions used in many underwater vehicle tracking algorithms. The mean predicted output is

$$\hat{y}_{k|k-1} = \sum_{i=0}^{2L} \eta_i^m \psi_{k|k-1}^i \tag{31}$$

where $\eta_i^m$is the weighted vector for the mean, and $\psi_{k|k-1}^i$ is the propagation of sigma points.

The covariance of the predicted output is given by

$$P_k^{yy} = R_k + \sum_{i=0}^{2L} \eta_i^c \left(\psi_{k|k-1}^i - \hat{y}_{k|k-1}\right)\left(\psi_{k|k-1}^i - \hat{y}_{k|k-1}\right)^T \tag{32}$$

In (32) R_k is the measurement covariance. The cross-covariance of the state and the output is given by

$$P_k^{xy} = \sum_{i=0}^{2L} \eta_i^c \left(\chi_{k|k-1}^i - \hat{x}_{k|k-1}\right)\left(\psi_{k|k-1}^i - \hat{y}_{k|k-1}\right)^T \tag{33}$$

The measurement update stage of the UKF is similar to that of the Kalman filter and the EKF. The measurement update stage is given by

$$K_k = P_k^{xy}\left(P_k^{yy}\right)^{-1} \tag{34}$$

In (34) K_k is the Kalman gain, and by

$$\hat{x}_k = \hat{x}_{k|k-1} + K_k\left(Z_k - \hat{y}_{k|k-1}\right) \tag{35}$$

In (35) $\hat{x}_k$ is the state estimate update. The error covariance update is then given by

$$P_k = P_{k|k-1} - K_k P_k^{yy} K_k^T \tag{36}$$

D. SIMULATED ANALYSIS OF THE UKF AND EKF POSITION-ESTIMATING TECHNIQUES

A simulation was conducted using the previous USBL measurements for the REMUS 100 AUV docking station. Dead reckoning measurements were simulated using the cross-track-error control and dead reckoning equations. A total of ten runs were used to evaluate the ability of the UKF and EKF in estimating the position of the vehicle. A

small bias associated with the heading was assumed and used for every run. The initial uncertainty of the vehicle with respect to the simulated USBL measurements was also assumed and used.

The docking error was regarded as the distance from the center of the entrance of the docking station to the longitudinal centerline of the AUV. Figure 18 illustrates how the error was measured. In Figure 18 the vehicle is on the surface and the docking station is shown as a white rectangular frame. The reader should note that this is an illustration for docking error measurement only. For an AUV to dock, the error (e) should be less than 0.35m. The size of the square entrance is 0.7m in height and 0.7m in breath, and 0.35m is the radius of the entrance.

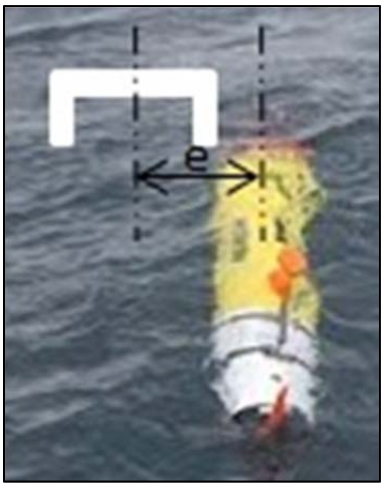

Figure 18. Docking Error Computation Illustration

Table 4 shows the results of the simulation. No docking success was achieved in any run; however, as expected, the UKF managed to position the vehicle much closer to the docking station than the EKF technique.

Table 4. Simulated UKF and EKF Undersea Docking Results

Runs	USBL Update rate in (Hz)	Bias in (% distance travelled)	Initial Uncertainty in (m)	UKF Docking error (m)	EKF Docking error (m)	Docking Success		
						REMUS	UKF	EKF
1	0.401	0.70%	10.8	4.323	4.331	No	No	No
2	0.299	1.00%	8.5	8.109	8.129	No	No	No
3	0.319	0.90%	11.4	2.908	2.911	No	No	No
4	0.428	0.60%	7.5	4.092	4.102	No	No	No
5	0.436	0.70%	6.7	3.913	3.924	No	No	No
6	0.252	0.60%	4.2	2.690	2.698	No	No	No
7	0.209	0.40%	3.0	5.629	5.651	No	No	No
8	0.351	0.60%	3.0	3.008	3.018	No	No	No
9	0.255	0.40%	3.3	2.916	2.925	No	No	No
10	0.343	0.50%	3.0	6.780	6.801	No	No	No
Average	0.329	0.64%	6.1	4.437	4.449			

Run 5 had a higher update rate; but the measurements were distributed poorly such that no docking success was possible using the UKF and EKF. Figure 19 shows the positions of the vehicle as represented by the curves associated with each estimating method. As expected, the UKF managed to position the vehicle a little closer to the docking station than the EKF.

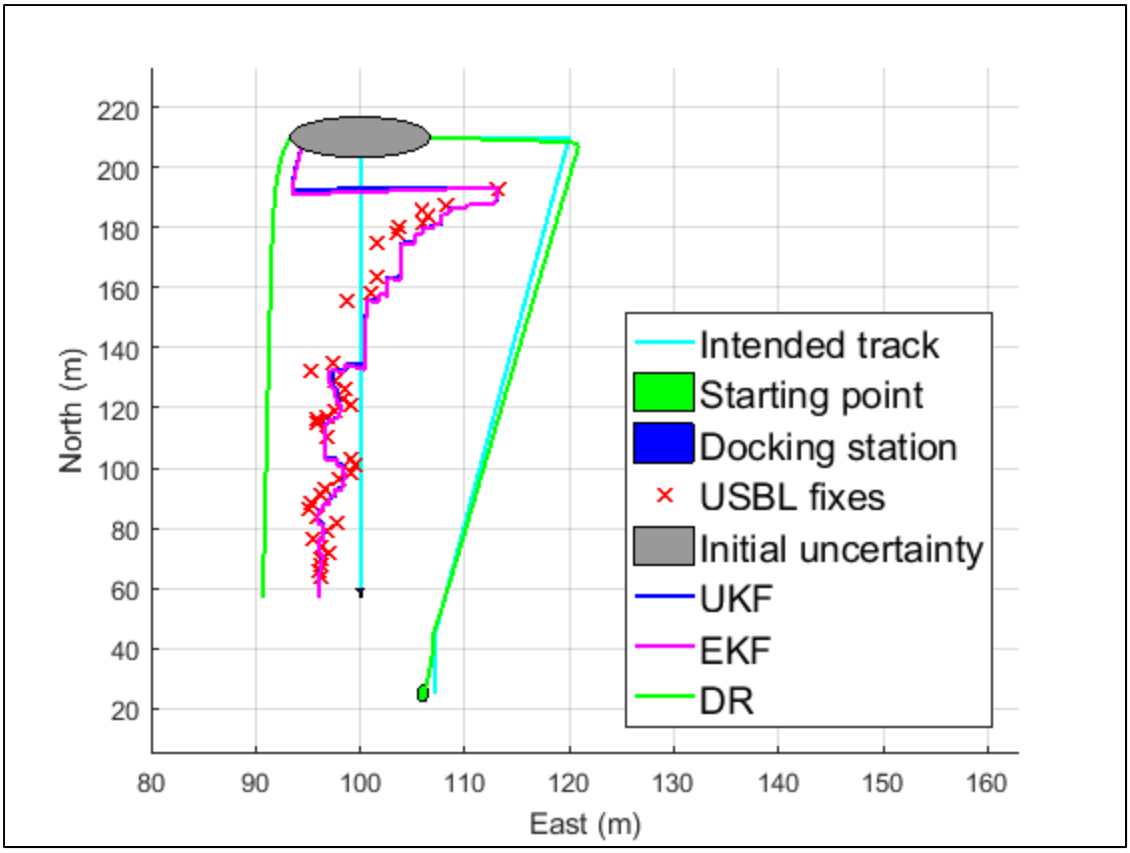

Figure 19. Run 5 with High Frequency Update Rate and Poor Docking Results

Run 7 had the lowest frequency update of USBL measurements. The results obtained from this run were as expected, owing to the low USBL sensor update rate. Figure 20 provides an illustration of the measurements' locations. As depicted, docking was impossible when the measurements were far from the intended track.

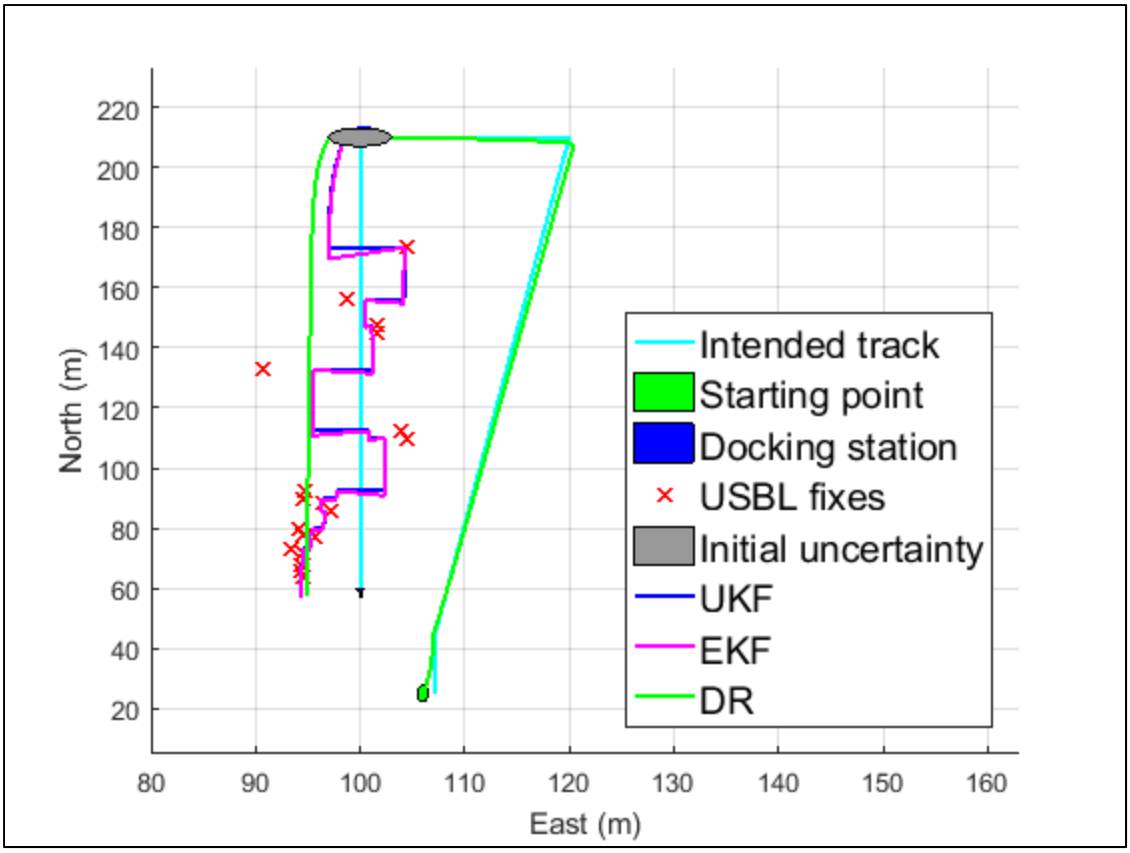

Figure 20. Run 7 with Lowest Update Rate and Poor Docking Results

THIS PAGE INTENTIONALLY LEFT BLANK

IV. MOVING HORIZON ESTIMATION WITH EPI-SPLINES

A. INTRODUCTION

In the last chapter the EKF and UKF were used for AUV position estimation. The performance was poor due to the sparse, erroneous, sporadic USBL measurements. In this chapter the Moving Horizon Estimation is presented as an alternative. It is the state estimation method that uses ideally all available observed system dynamics measurements as constraints to estimate the state of a nonlinear or constrained system through solving an optimization problem [21]. The strength of the approach is that it handles the constraints in a more systematic way. Furthermore a new, modified MHE has been developed. It leverages the fact that over relatively short time horizons the AUV trajectory has limited positional uncertainty. This can be combined with the USBL measurements to provide a more accurate, reliable position solution. The technique utilizes an epi-spline technique for non-linear least squares estimation of the moving horizon estimation. Epi-splines are "the newly developed piecewise polynomial functions described by the finite number of parameters, which are exceptionally flexible." Royset and Wets [17]. They are useful for their ability to incorporate both soft and hard constraints Royset and Wets [31].

The EKF and UKF aimed to solve (37), the maximum likelihood estimate for the systems of equations (1) and (2).

$$x_k^+ = \arg\max_{x_k} p(x_k|z_0, \dots, z_k) \tag{37}$$

where $p(x_k|z_0, \dots, z_k)$ is the probability that the system state is x_k given measurements $z_0, \dots, z_k$. As shown in Haseltime and Rawlings [32], the MHE maximizes the joint probability for the trajectory of the state values such that

$$x_k^+, \dots, x_T^+ = \arg\max_{x_k,\dots,x_T} p(x_k, \dots, x_T|z_0, \dots, z_k) \tag{38}$$

According to [32], for constrained nonlinear systems, logarithmic transformation of (37) is computationally easy:

$$\arg\max_{x_k,\dots,x_T} -\log p(x_k, \dots, x_T|z_0, \dots, z_k) = \arg\max_{x_k,\dots,x_T} p(x_k, \dots, x_T|z_0, \dots, z_k) \tag{39}$$

because, by assuming that the *a priori* state estimate is a $N(x_0, \sum_0)$ distributed noise, minimization of (39), which is subject to the nonlinear model (1), gives rise to a least-squares optimization:

$$\Phi_T = \min_{x_k,\ldots,x_T} \Gamma(x_0) + \sum_{k=0}^{T-1} w_k^T Q_k^{-1} w_k + \sum_{k=0}^{T} v_k^T R_k^{-1} v_k \tag{40}$$

$$Such\ that: \Gamma(x_0) = (x_0 - \hat{x}_0)^T \Sigma^{-1} (x_0 - \hat{x}_0) \tag{41}$$

$$\hat{x}_{k|k-1} = F(\hat{x}_{k-1}, u_{k-1}) + w_k \tag{42}$$

$$Z_k = h(\hat{x}_{k-1}) + v_k \tag{43}$$

$$x \in X, w \in W, v \in V \tag{44}$$

Equations (40) through (43) are collectively called the full information problem, and *X*, *W* and *V* contain the values of the system state, system disturbance, and measurement disturbance, respectively [32]. The *X* component contains values for the vehicle constraints such as turn rate, pitch rate, and velocity [32]. This problem is difficult to solve due to its computational complexity. For this reason, the nonlinear least squares optimization technique is applied to solve the full information problem.

In order to use the MHE approach for real-time applications, the optimization process should be quick and accurate; therefore, the epi-splines were used for the optimization process. Royset and Wets [33] derived the equations used for the epi-splines MATLAB programming code in this thesis. The equations used in this thesis were extracted from Horner and Mqana [1], Royset and Wets [17], [31] and [33], and Peter Tydingco [34], and they appear in the following paragraphs. The epi-splines are defined as the piecewise polynomials with extended, real valued, lower semi-continuous functions on R^n and defined by the polynomial order, the number of partitions (S) and the mesh $m = \{m_k\}_{k=0}^{S}$ [1]. See Horner and Mqana [1] for an in-depth analysis of the epi-splines.

During the optimization process, the epi-splines produce the vehicle's trajectory from the vehicle state. The next step of the optimization process fits the vehicle trajectory to the USBL measurements accordingly [1]. The first step of the optimization process with epi-splines is described as follows:

$$\underset{\lambda}{\text{Min}}\frac{1}{n}\sum_{i=1}^{n}\lambda_i \tag{45}$$

$$\text{where } f(d_i) - \left[a_0^{k_1} + a_1^{k_1}d_i + a_2^{k_1}d_i^2\right] \leq \lambda_i, \forall i = 1, 2, \ldots n$$

$$\left[a_0^{k_1} + a_1^{k_1}d_i + a_2^{k_1}d_i^2\right] - f(d_i) \leq \lambda_i, \forall i = 1, 2, \ldots n$$

$$a_0^k + a_1^k m_k + a_2^k m_k^2 = a_0^{k+1} + a_1^{k+1} m_k + a_2^{k+1} m_k^2$$

$$a_1^k + 2a_2^k m_k = a_0^{k+1} + 2a_2^{k+1} m_k, \forall i = 1, 2, \ldots S - 1$$

$$u \leq \lambda \leq l$$

The epi-splines are piecewise polynomials at every segment with $f(d) = \left[a_0^{k_1} + a_1^{k_1}d_i + a_2^{k_1}d_i^2\right]$ representing the polynomial for vehicle data and $\lambda_i = |f(d_i) - \hat{f}(d)|$ representing the absolute value of the difference between the vehicle data and the predicted vehicle data. The constraints enumerated in (45) are used to minimize the average error between the vehicle data points and the fitted curve. The first and second constraints in (45) are for minimizing the error associated with the objective function. The third constraint is for ensuring continuity of the function. The fourth constraint is for ensuring continuity of the derivative of the function. The fifth constraint sets the upper and lower boundaries for the absolute difference between the vehicle data and the predicted vehicle data. The second step of the optimization minimizes the error between the USBL measurements and the curve fitted by the epi-spline optimization process. The resulting output is the MHE trajectory that represents the optimal estimate of the path of the vehicle.

B. MOVING HORIZON ESTIMATION WITH EPI-SPLINE SIMULATION

The MHE with epi-splines was applied to past docking station runs of the real REMUS 100 AUV. The AUV's dead reckoning measurements were used as constraints for the epi-splines to produce the trajectory of the AUV. The nonlinear least squares method was then used to fit the trajectory of the AUV through the available USBL measurements in accordance with the covariance of the dead reckoning system and USBL measurements.

The MHE begins after the window has the first five USBL measurements. Figure 21 illustrates how the MHE with epi-splines works. The MHE with epi-splines uses the measurements in the window and produces a curve for the estimated states associated with the measurements in the window. The MHE is applied only when an additional measurement has been obtained. The window is fixed to the first USBL measurement and extends every time there is a new USBL measurement. The process repeats until the epi-splines are applied in the window containing all USBL measurements.

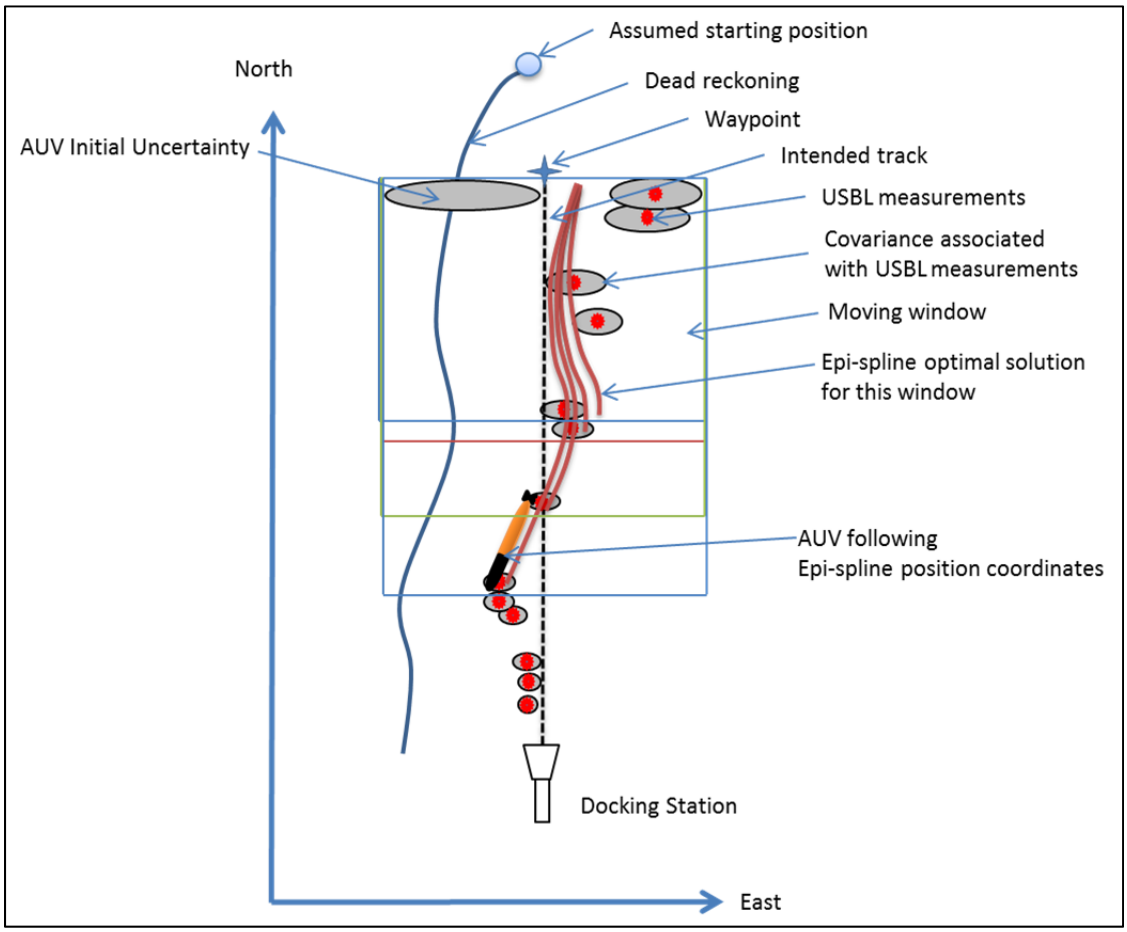

Figure 21. Illustration of Moving Horizon Estimation with Epi-Spline

Every time the epi-splines produce the estimated means curve, the curve rotates using the covariance associated with the USBL measurements and the covariance associated with the dead reckoning measurements.

Figure 22 shows how the epi-splines with nonlinear least squares fit the curve for the means of the available USBL measurements and in accordance with the dynamics of the vehicle in the current window.

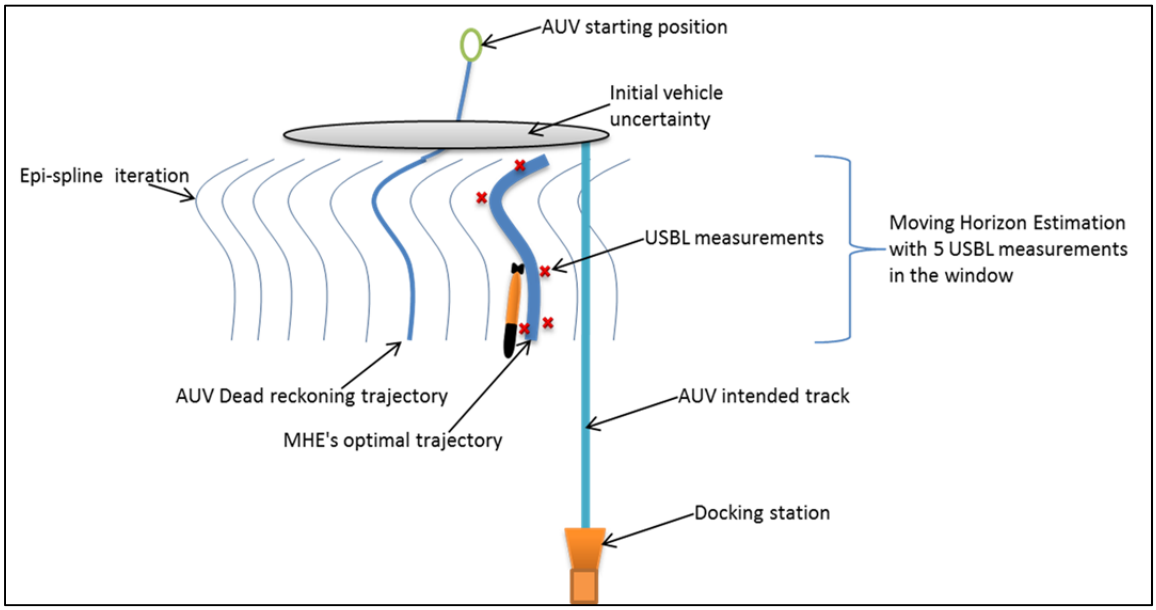

Figure 22. Illustration of How the Optimal Curve Is Fitted

Notably, the thick blue curve has the same trajectory as the curve for a dead reckoning AUV shown in Figure 22. While the covariance associated with dead reckoning measurements grows linearly over distance traveled, the covariance associated with the USBL measurements drops linearly as they get closer to the docking station.

For this analysis, the vehicle started at a position just before it could receive the USBL measurements. During the complete run of the REMUS 100 AUV, the vehicle starts closer to the docking station and travels about 150 m dead reckoning before receiving USBL measurements. When the vehicle approaches the zone where it can receive USBL measurements, the accumulated dead reckoning error is high. This accumulated error is used in this thesis as the initial vehicle uncertainty. Sometimes the vehicle moves closer to the zone where the chances of receiving USBL measurements are high, making the initial uncertainty of the vehicle small.

The initial uncertainty is also used as the variance associated with dead reckoning measurements when rotating the epi-splines results according to the covariance associated with USBL and dead reckoning measurements. Figure 23 illustrates the rotation of the curves produced by the epi-splines for every window. The curves start by settling in between the dead reckoning and USBL measurements, but as the window stretches, the curves move away from the dead reckoning measurements and closer to the USBL measurements.

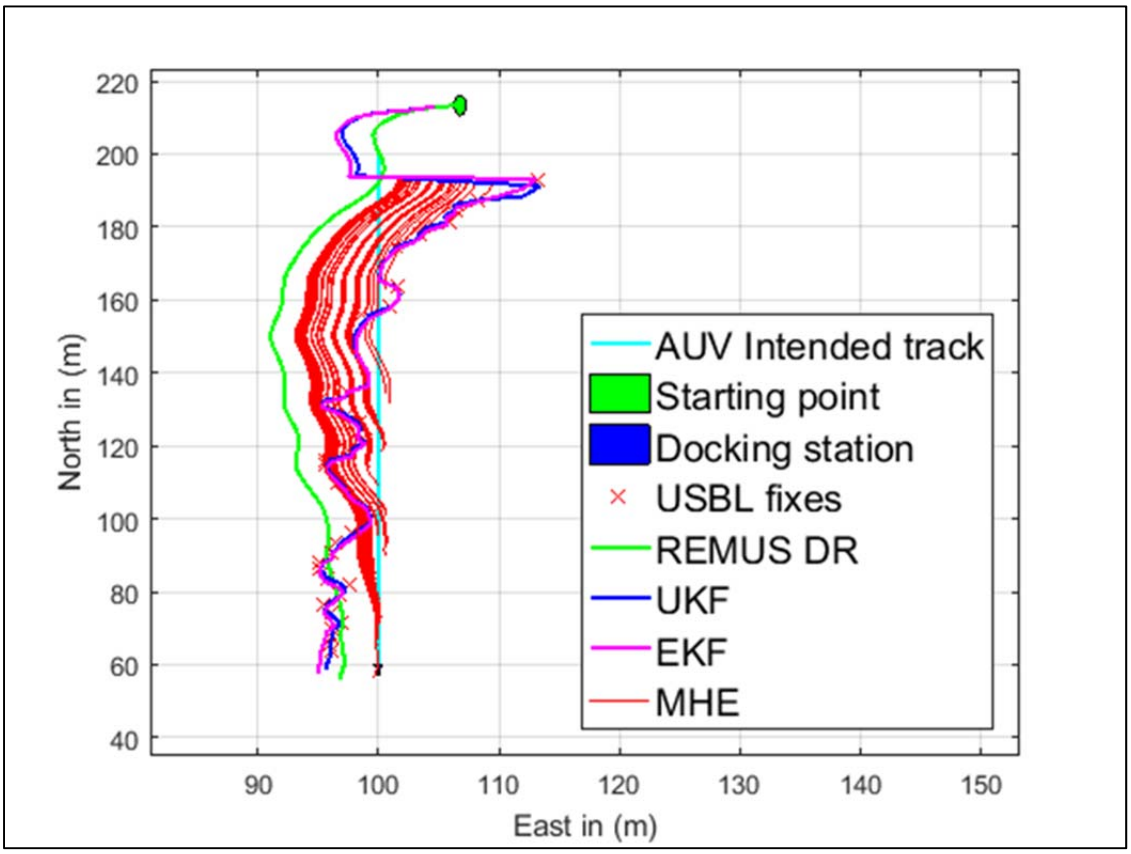

Figure 23. MATLAB Results Showing the Epi-Spline Optimal Solution in Every Window

Figure 24 further illustrates the rotation of the curve for the estimated means and its deviation from the dead reckoning curve as the vehicle approaches the docking station.

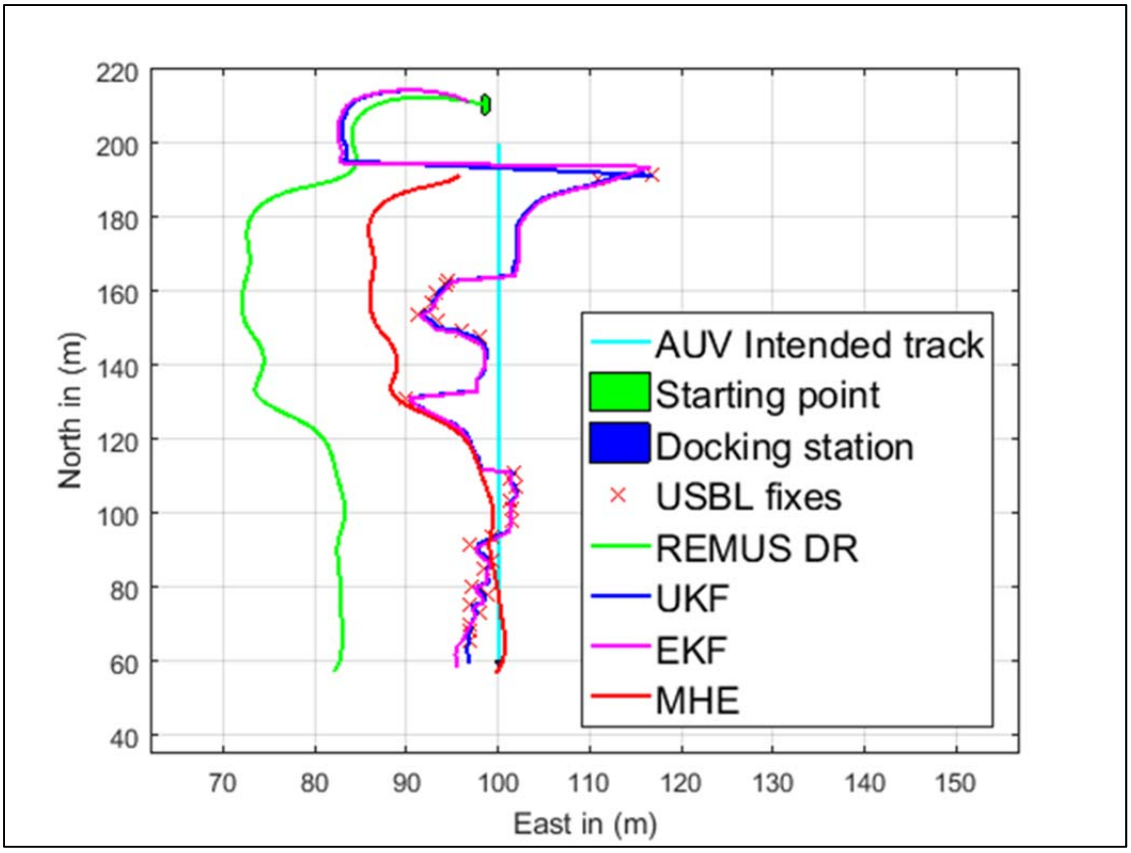

Figure 24. Final MHE Results

C. MOVING HORIZON ESTIMATION WITH EPI-SPLINE ALGORITHM

The algorithm used for the MHE is illustrated in Table 5. The inputs to the epi-splines algorithm are the MHE window size (MHE_{ws}) , the system state for the window size (χ_T), the covariance for the system state of the window size (P_T), the constraints associated with vehicle dynamics as given by the measurement vector (Z_k), and the USBL measurements in the window size (Z_{USBL}).

For accurate approximation results, the MHE horizon should contain all the measurements; however, this requires significant computational memory from the system [21]. The window size used for this thesis started with five USBL measurements, and it kept stretching to accommodate new measurements until all the USBL measurements fit within the window.

The methodology for propagating the vehicle from the starting position to the zone where USBL measurements are available is either the UKF or EKF. The MHE starts when the USBL measurements are available. The threshold is set to a small constant value.

Table 5. Illustration of the Algorithm Used for the MHE with Epi-Splines

Input	$\chi_T,\ P_T, Z_k, Z_{USBL}, MHE_{ws}$
Output	$\chi_{epi},\ P_{epi}$
Initialization	$x_0,\ P_0, MHE_{ws}, \mu, Threshold$
Computation of input parameters	$\chi_T = [x_n \vert x_{n+1} \vert \dots x_k]$ $P_T = [P_n \vert P_{n+1} \vert \dots P_k]$ $Z_{USBL} = [z_{USBL\,n} \vert z_{USBL\,n+1} \vert \dots z_{USBL\,k}]$ $Z_k = [z_n \vert z_{n+1} \vert \dots z_k]$ $nz = columns[Z_k]$

Beginning the iteration with epi-splines	**if** $(nz > MHE_{ws})$
	$\left[\chi_{epi},\ P_{epi}\right] = epi\_spline(\chi_T,\ P_T, Z_k, Z_{USBL})$
	if $(\mu < Threshold)$
	$(x_{k-N}, x_{k-N+1}, \dots x_k)^T = \chi_{epi}$
	$(P_{k-N}, P_{k-N+1}, \dots P_k)^T = P_{epi}$
	else
	$Z_{USBL} = [z_{USBL\,n+1} \vert, \dots \vert z_{USBL\,k}]$
	end if
	end if

The optimization process takes place and provides the estimated state as long as the optimization error is less than the set threshold; otherwise, the bad measurement is left unused by the optimization, and the window extends to accept a new measurement. The optimization process continues until all USBL measurements have been used. The ability of epi-splines to incorporate soft and hard constraints makes them favorites in optimization problems. Other epi-spline advantages include their applicability in piecewise functions of any space, their requirement of one lower-semicontinuous input boundary, and their ability to approximate every lower-semicontinuous function to any accuracy.

THIS PAGE INTENTIONALLY LEFT BLANK

V. RESULTS AND ANALYSIS

A. METHODOLOGY

The EKF, UKF and MHE with epi-splines were evaluated on their capabilities of estimating the position of the REMUS 100 AUV in the future using the current state of the system. Past docking mission runs of the AUV were used to evaluate these position estimating techniques. To measure the effectiveness of each of these techniques, the final location of the REMUS 100 AUV was computed relative to the center of the entrance of the docking station. The distance from the center of the docking station entrance to the edge is 0.35 m in all directions. If the vehicle's final position is within 0.35 m of the center of the entrance, docking is considered successful. The reader is referred to Figure 18 for an illustration of the docking error metric.

Sometimes the USBL measurements become available, and sometimes they do not. The USBL update rate is computed as follows:

$$USBL\ Update\ Rate(in\ Hz) = \frac{no.\ of\ USBL\ measurements \times average\ forward\ velocity}{distance\ between\ the\ docking\ station\ and\ the\ last\ waypoint}$$

In some runs, the update rate is very small, but the measurements are packed closer to the intended track. A total of 19 previous REMUS 100 AUV docking station runs were used for this evaluation. During these runs, the REMUS 100 AUV managed to dock only once during actual in-water testing. The position estimating techniques were evaluated to determine whether they would have managed to dock the vehicle by placing within the boundaries of the docking station entrance. The results for this evaluation are shown in the next section.

B. PREVIOUS REMUS 100 DOCKING STATION RUNS – EVALUATION RESULTS AND ANALYSIS

Figure 25 shows the REMUS 100 AUV's dead reckoning trajectory for an underwater docking station run that was conducted in Monterey Bay, California in 2014. The vehicle attempted to dock during its first trial but missed the docking station. The

vehicle made its second attempt and docked successfully. Shown in the image is the combination of the two trajectories in blue. The red crosses represent the USBL measurements received during the first trial, and the black dots are USBL measurements received during the second trial. The vehicle started at the position marked in green as shown. The docking station was close to the starting point. The AUV's intended track was the straight cyan line. Notably, the REMUS 100 AUV deviates from its path as the vehicle's dead reckoning measurement error grows linearly.

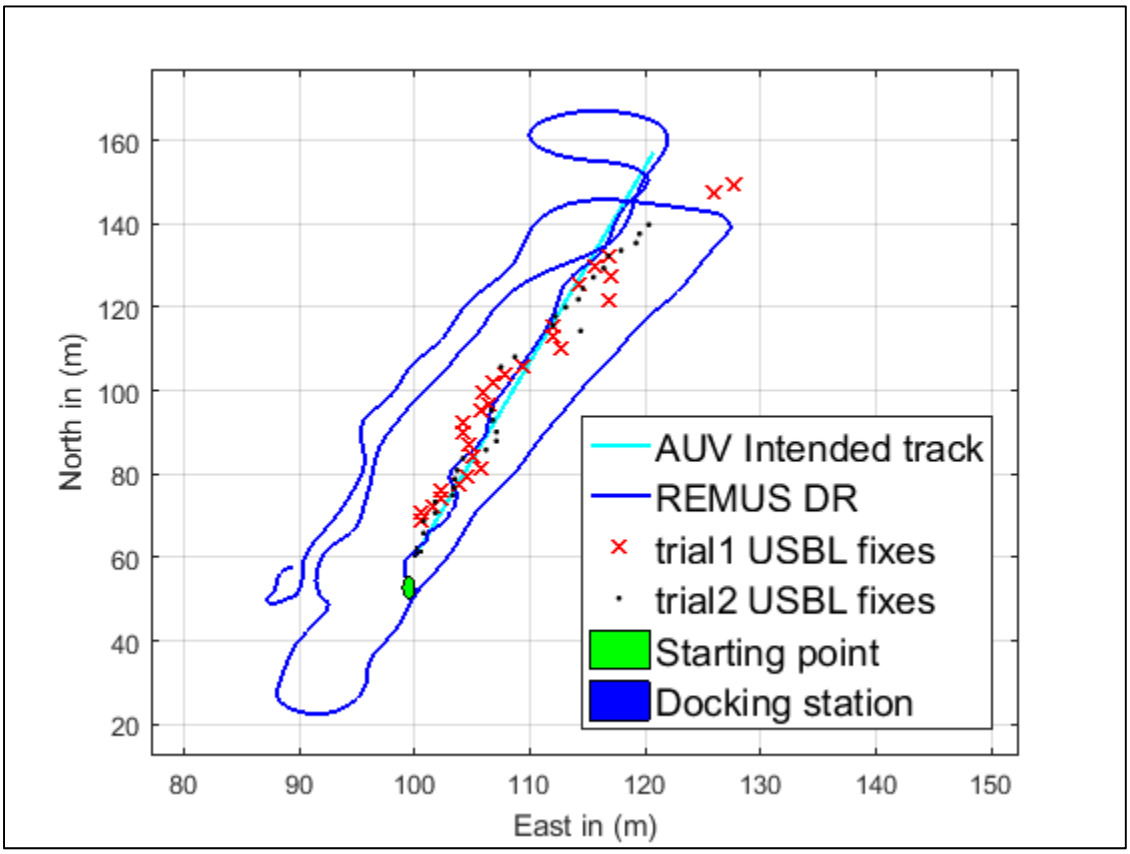

Figure 25. MATLAB Plot of REMUS 100 Dead Reckoning for Two Trials

The same illustration is shown in Figure 26. This diagram has been extracted from the REMUS 100 AUV software (VIP).

In Figure 26, the dead reckoning trajectory is shown in blue arrows; the yellow arrows indicate the USBL measurements available to the vehicle during the two trials. The docking station is indicated with the cyan star at the lower end of the intended track line. This docking station run corresponds with Runs 16 and 17 in Table 6.

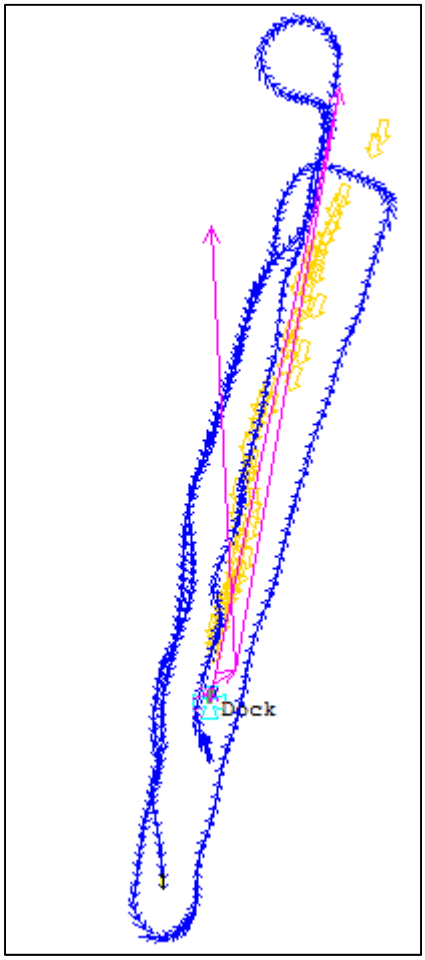

Figure 26. REMUS 100 Dead Reckoning Trajectory from VIP Softwear

Table 6 shows the results of the evaluation conducted using previous docking station runs of the REMUS 100. As the table indicates, the MHE managed to dock the vehicle on five runs while the UKF and EKF only managed to dock the vehicle twice. The UKF and EKF docked the vehicle on the same run that the REMUS 100 managed to dock during its real mission in water. The MHE did not dock on this run, but it placed the vehicle close to the docking station.

Table 6. Results Obtained from Previous REMUS 100 Mission Runs Performed Using the UKF, EKF and MHE

Runs	USBL Update rate	Initial Uncertainty	UKF	EKF	MHE	Docking Success			
	(Hz)	(m)	Docking error (m)	Docking error (m)	Docking error (m)	REMUS	UKF	EKF	MHE
1	0.401	20.80	3.93	4.65	0.46	No	No	No	No
2	0.299	16.00	8.52	9.22	0.58	No	No	No	No
3	0.319	22.40	3.26	4.51	0.46	No	No	No	No
4	0.428	15.80	4.20	5.40	0.18	No	No	No	Yes
5	0.436	13.70	4.23	4.87	0.08	No	No	No	Yes
6	0.252	8.20	3.38	3.84	0.31	No	No	No	Yes
7	0.209	2.50	5.53	6.32	4.82	No	No	No	No
8	0.351	0.00	3.09	4.01	0.98	No	No	No	No
9	0.255	2.60	3.24	4.41	1.22	No	No	No	No
10	0.343	0.00	6.79	7.20	0.43	No	No	No	No
11	0.429	3.70	2.48	3.38	0.07	No	No	No	Yes
12	0.346	6.80	1.53	2.76	0.44	No	No	No	No
13	0.344	4.60	2.22	2.96	0.79	No	No	No	No
14	0.307	5.80	1.96	3.35	0.28	No	No	No	Yes
15	0.373	8.10	1.37	3.20	1.73	No	No	No	No
16	0.285	9.10	0.23	0.28	0.50	Yes	Yes	Yes	No
17	0.501	7.50	0.72	0.53	0.43	No	No	No	No
18	0.346	15.10	1.27	0.07	2.70	Yes	No	Yes	No
19	0.283	20.00	0.13	0.50	1.60	Yes	Yes	No	No
Average	0.336	9.62	3.06	3.76	0.95				

The average docking error associated with the MHE is relatively small compared to the EKF and UKF.

In Run 2, the vehicle position was estimated very far from the docking station using UKF and EKF techniques, but the MHE located it about 0.58 m away from the docking station. The depiction of this run is shown in Figure 27. The UKF and EKF followed the position of USBL measurements with small consideration of the vehicle dynamics due to the tuning of the covariance associated with the system model and the covariance associated with the measurement model.

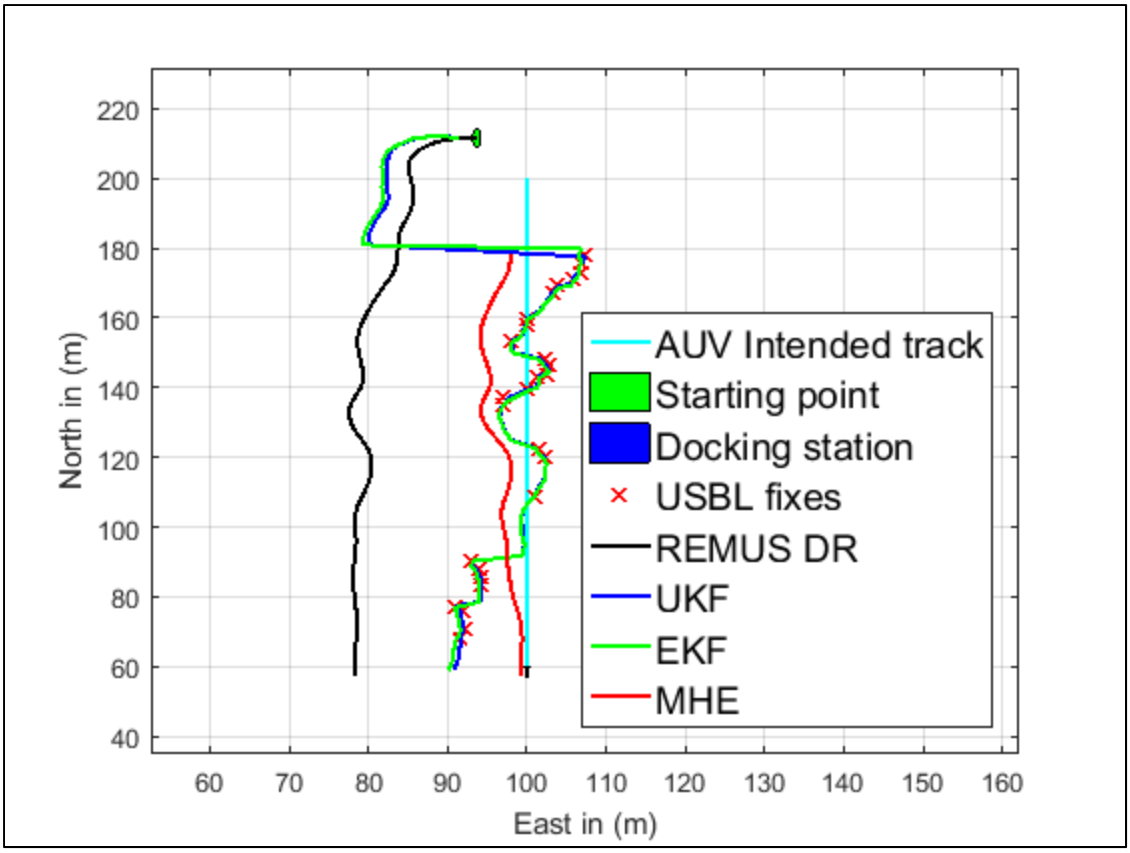

Figure 27. Run 2 Illustrating the Worse Performance by the UKF, EKF, and FBS Techniques

In Run 3, the vehicle had high initial uncertainty about the USBL measurements, but the performance from all techniques was better than some of the runs with low levels of initial uncertainty. Figure 28 shows the performance of these techniques under the vehicle's high uncertainty about the USBL measurements.

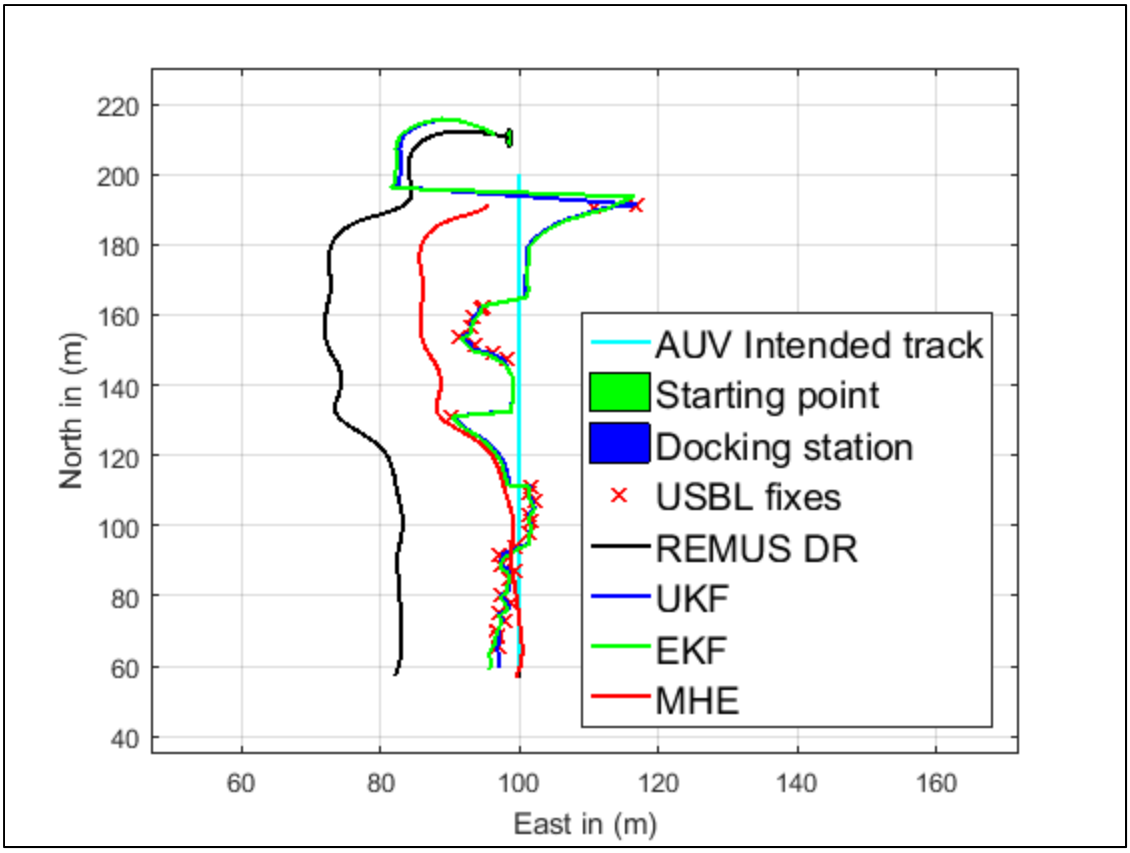

Figure 28. Run 3 Illustrating UKF, EKF and MHE Performance at a High Level of Initial Uncertainty

In Run 4, the USBL sensor update rate is the highest for the runs during which the REMUS vehicle did not dock. Analysis finds that the vehicle could have docked if it had been guided by the MHE technique. Figure 29 depicts this finding.

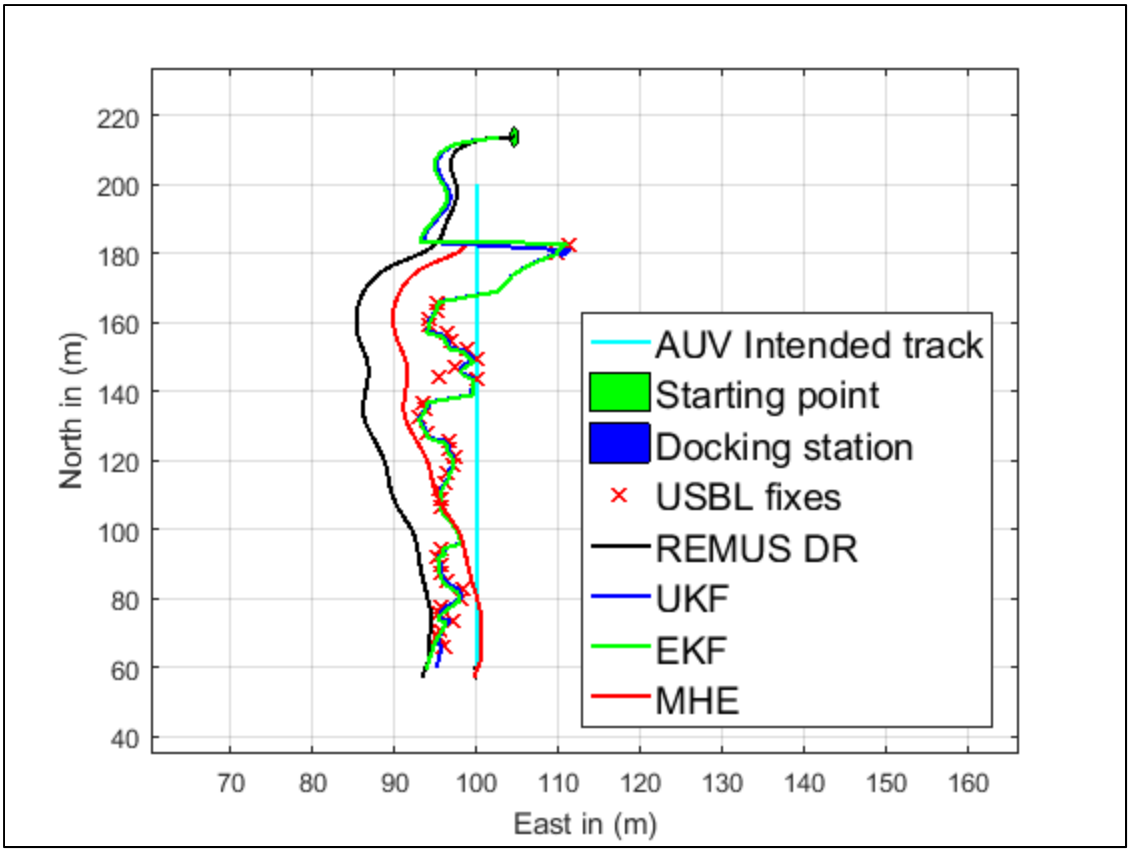

Figure 29. Run 4 Showing MHE Docked

Run 14 had a low frequency update rate, but MHE technique managed to dock. Figure 30 illustrates this docking. Once again, the EKF and UKF tracked the USBL measurements with small consideration of the vehicle dynamics due to the tuning of the covariance associated with the system model and the covariance associated with the measurement model.

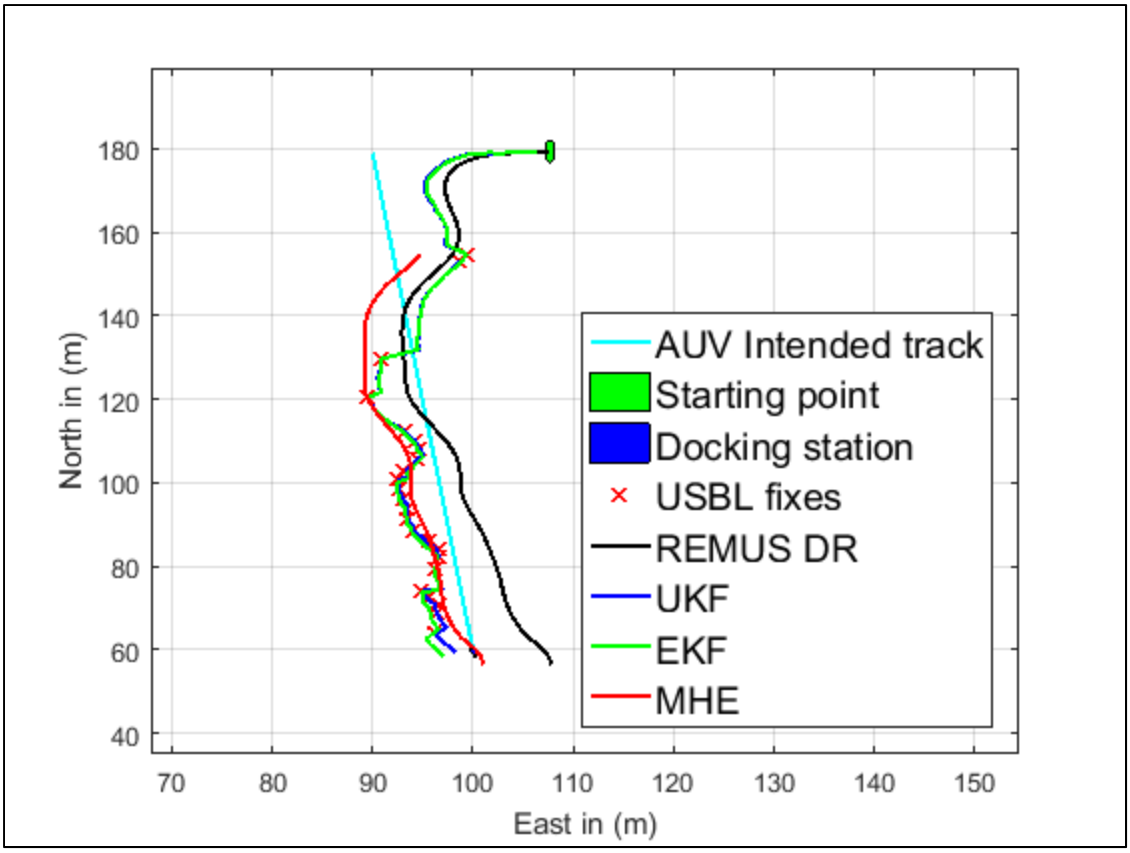

Figure 30. Run 14 Showing MHE Docked

In Run 16, the REMUS vehicle docked, which means the USBL measurements were good and directed the vehicle into the docking station. This is confirmed by docking with the UKF and EKF because they are good at tracking the measurements. In this run, the MHE did not dock. This was expected because MHE considers the dynamics of the vehicle; this time, the MHE techniques failed, but managed to place the vehicle within 0.5m from the center of the docking station. The equation used to combine the effect of the vehicle dynamics and the USBL measurements is as follows:

$$y_{optml\ mhe} = \frac{\sigma_{DR}^2 y_{mhe}}{\sigma_{DR}^2 + \sigma_{USBL}^2} + \frac{\sigma_{USBL}^2 y_{DR}}{\sigma_{DR}^2 + \sigma_{USBL}^2} \quad (46)$$

In (46) $y_{optml\ mhe}$ is the East (y) coordinate of the position of the vehicle as computed by the MHE with epi-splines method, σ_{DR} is the uncertainty associated with the dead reckoning measurements at that specific location, y_{mhe} is the output of the MHE with epi-splines method before considering the covariance associated with the dead reckoning

measurements and with the USBL measurements. In (46) y_{DR} is the East (y) component of the dead reckoning position of the vehicle while σ_{USBL} is the covariance associated with the USBL measurements. The covariance associated with the dead reckoning measurements grows linearly with the distance travelled while the covariance associated with the USBL measurements decreases linearly as the vehicle gets closer to the docking station but cannot be zero because the USBL measurements normally end at about 5 m away from the docking station.

As the vehicle moves closer to the docking station the $y_{optml\,mhe}$ tends to move away from the dead reckoning position of the vehicle due to (46). This becomes a challenge to the MHE especially when the USBL measurements are on the intended track; the MHE with epi-spline $y_{optml\,mhe}$ tends to be a little off from the intended track unlike the EKF and UKF. Figures 31 and 32 provide the illustration of this situation. In this image, the measurements are on the intended track as a result, EKF and UKF managed to dock but MHE with epi-spline went a little off from the docking station.

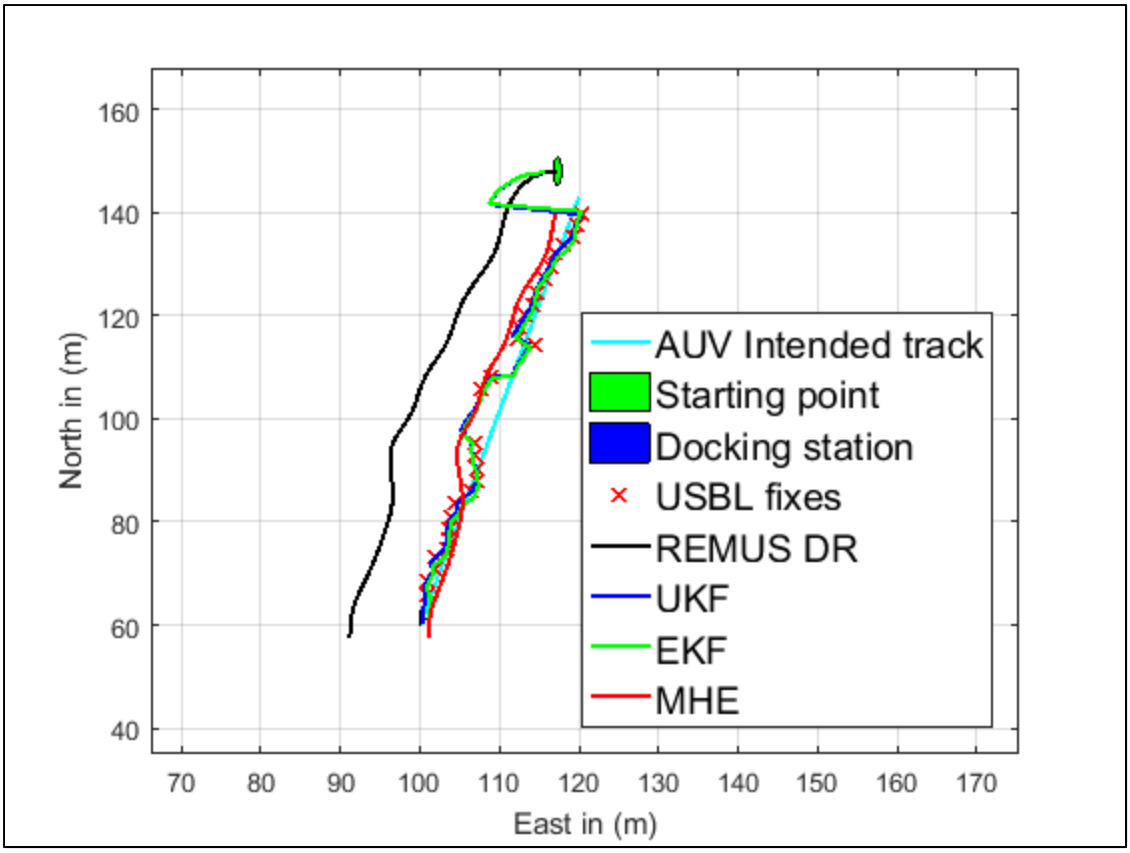

Figure 31. Run 16 Showing UKF and EKF Docked while MHE Failed to Dock

In Run 19, the REMUS 100 AUV docked successfully. The UKF also managed to dock as expected. As discussed in Run 16's explanation, the MHE with epi-splines missed the docking station by a small error. Figure 32 shows the distribution of the USBL measurements and the final estimated positions of the vehicle for other position estimating techniques.

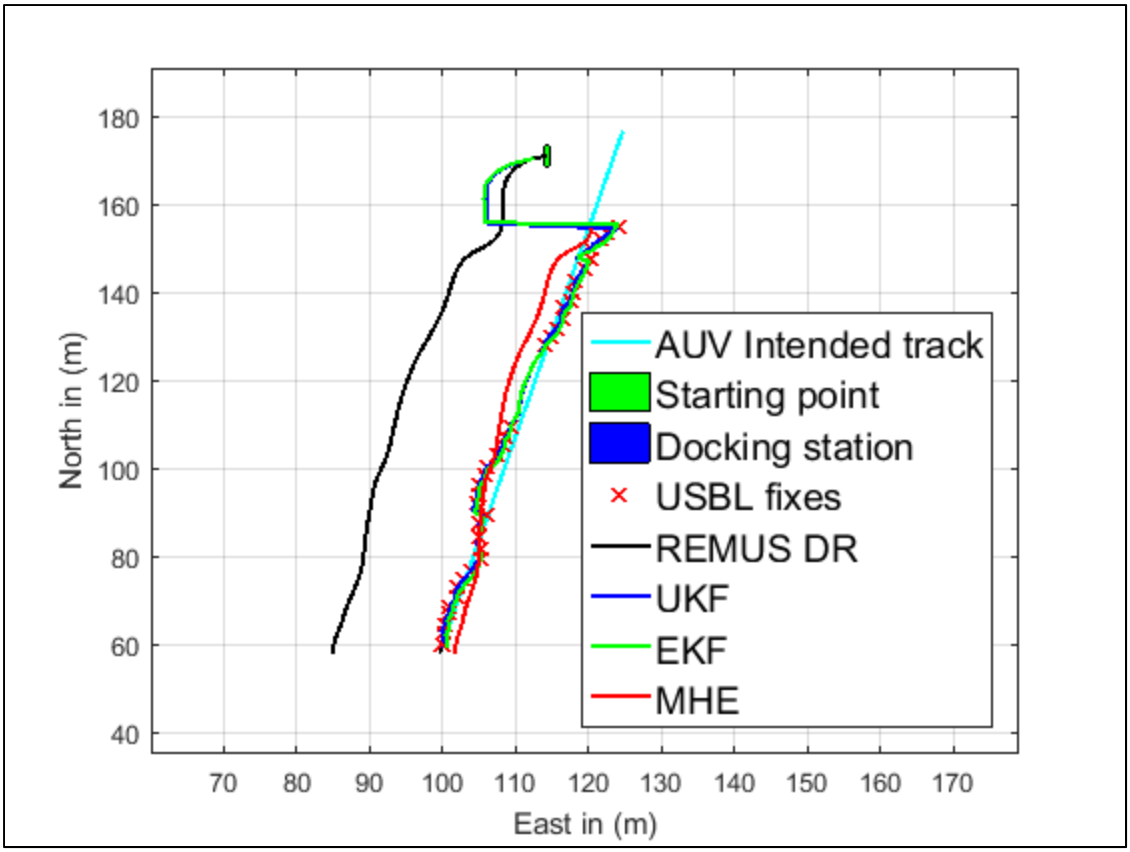

Figure 32. Run 19 Showing REMUS 100 Docked Successfully

THIS PAGE INTENTIONALLY LEFT BLANK

VI. POSITION ESTIMATION USING FBS

A. INTRODUCTION

After evaluating the EKF and the UKF position estimating methods and obtaining unsatisfactory results, the forward and backward smoothing (FBS) position estimating method was introduced. The FBS is a technique applied to the measurements to obtain an optimal smoothed estimate [23]. "The information filter is defined as the implementation of the Kalman filter that propagates the inverse of the covariance instead of propagating the covariance" [23]. Mathematically, the information filter is related to the Kalman filter by

$$I_{inf} = P^{-1} \tag{47}$$

In (47) I_{inf} is the certainty in the state for the information filter and P^{-1} is the inverse of the state covariance for the forward smoothing techniques [23]. The information filter is recommended for use in the backward smoothing technique where the knowledge of the state is uncertain or unavailable. This is due to the fact that the information filter is mathematically defined with zero confidence, $I_{inf} = 0$, where the uncertainty of the forward smoothing algorithm approaches infinity, $P_k \to \infty$ [23]. The equations used to implement the backward smoothing as detailed in [23] are as follows:

$$I_{inf}{}_k^- = Q^{-1} - Q^{-1}\emptyset_k \left(I_{inf}{}_{k-1}^+ + \emptyset_k{}^T Q^{-1}\emptyset_k\right)^{-1} \emptyset_k{}^T Q^{-1} \tag{48}$$

$I_{inf}{}_k^-$ is the certainty associated with the state at the previous time step.

Q^{-1} is the inverse covariance for the process.

$\emptyset_k$ is the continuous state transition matrix as defined by $\emptyset = e^{Adt}$.

$I_{inf}{}_{k-1}^+$ is the certainty associated with the state at the previous time step.

$$I_{inf}{}_k^+ = I_{inf}{}_k^- + H_k^T R^{-1} H_k \tag{49}$$

$I_{inf}{}_k^+$ is the certainty associated with the state at one time step into the future.

H_k^T is the transpose of the Jacobian obtained by linearizing the measurement function h around the current state.

R^{-1} is the inverse covariance for the measurements.

$$K_k = \left(I_{inf}{}_k^+\right)^{-1} H_k^T R^{-1} \tag{50}$$

K_k is the Kalman gain.

$$\hat{x}_k^- = \emptyset_k \hat{x}_{k-1}^+ \tag{51}$$

$\hat{x}_k^-$ is the predicted state.

$\hat{x}_{k-1}^+$ is the state at previous time step.

$$\hat{x}_k^+ = \hat{x}_k^- + K_k(Z_k - H_k \hat{x}_k^-) \tag{52}$$

$\hat{x}_k^+$ is the smoothed estimate at one time step into the future.

Z_k is the observed state.

The FBS technique results in two optimal estimates. The first estimate is obtained using UKF running forward in time from the first to the fifth USBL measurements in the interval of ten measurements. The second estimate is obtained using an information filter running backward in time from the last USBL measurement in the current window to the fifth measurement in the current window size for the first nine USBL measurements. The two estimates are combined according to their Kalman gains and their covariances. The equations used are as follows:

$$P_m = \left[\left(P_{fm}^+\right)^{-1} + (P_{bm}^-)^{-1}\right]^{-1} \tag{53}$$

P_m is the optimal smoothed estimate covariance.

$\left(P_{fm}^+\right)^{-1}$ is the inverse of the forward smoothed estimate which is equal to $(P_k)^{-1}$.

$(P_{bm}^-)^{-1}$ is the inverse of the backward smoothed estimate which is equal to $I_{inf}{}_k^+$.

$$\hat{x}_m = P_m\left(I_{fm}^+ \hat{x}_{fm}^+ + I_{bm}^- \hat{x}_{bm}^-\right) \tag{54}$$

$\hat{x}_m$ is the optimal smoothed estimate.

I_{fm}^+ is the certainty of the forward smoothing technique.

I_{bm}^- is the certainty of the backward smoothing technique.

$\hat{x}_{fm}^+$ is the forward smoothed estimate.

$\hat{x}_{bm}^{-}$ is the backward smoothed estimate.

The resultant smoothed estimate was utilized as an optimal estimate by an ordinary UKF that updated the state using only the smoothed estimates. The window of measurements expanded as new USBL measurements were received until all the available measurements were used to estimate the state of the system. Figure 33 illustrates how the FBS was implemented. This image shows an uncertainty associated with the USBL measurements at the start of the region where the vehicle receives USBL measurements. The image also shows an uncertainty associated with the starting point of the backward smoothing as well as the red dot representing a smoothed estimate. The image also shows the window with 9 USBL measurements. Two REMUS 100 AUV positions are shown, representing a solution calculated from the dead reckoning measurements only, and the solution calculated from the FBS-smoothed estimates.

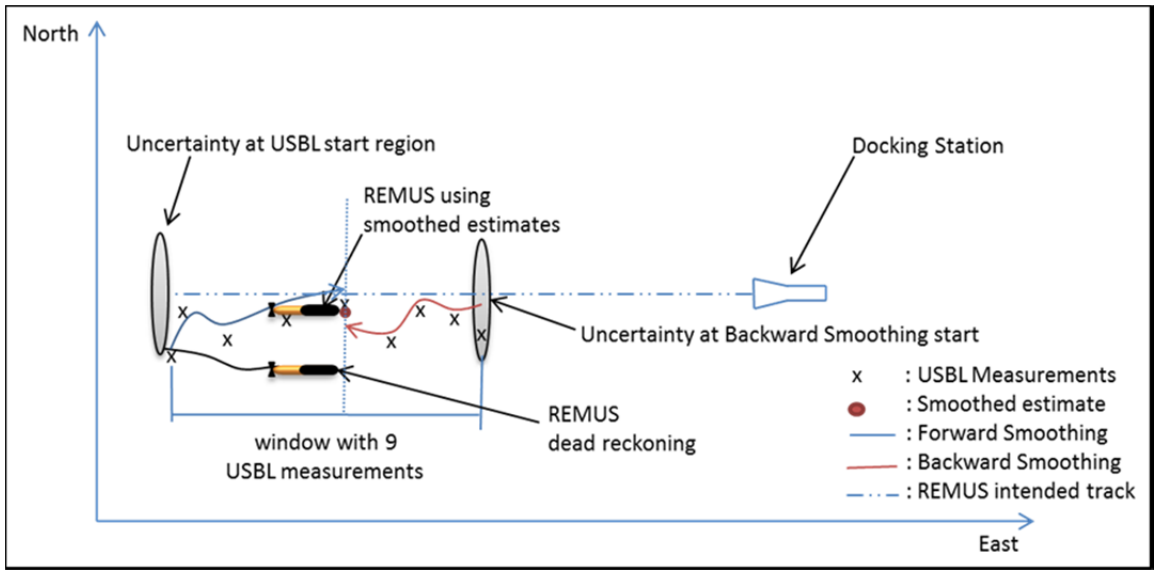

Figure 33. Illustration of Forward and Backward Smoothing Technique

The algorithm used for the FBS technique is illustrated in Table 7. In this table, N is the number of USBL measurements and $m = N/2$ is the stop position for both techniques.

Table 7. FBS Technique Algorithm

Information Filter Input	$\hat{x}_k^-, I_{inf}{}_k^-, Z_k, N \;\; k = N{:}\, m$
UKF Input	$\hat{x}_{k\|k-1}, P_{k\|k-1}, Z_k, N \;\; k = 1{:}\, m$
Information Filter Output	$I_{bm}^-, \hat{x}_{bm}^-$
UKF Output	$I_{fm}^+, \hat{x}_{fm}^+$
FBS output	x_m, P_m
Information Filter initialization	$\hat{x}_{k-1}^+, I_{inf}{}_{k-1}^+, m$
UKF initialization	$\hat{x}_{k-1}, P_{k-1}, m$
Core steps	**for** $(k = 1{:}\, m)$ $[I_{fm}^+, \hat{x}_{fm}^+] = UKF(\hat{x}_{k\|k-1}, P_{k\|k-1}, Z_k)$ **end** for **for** $(k = N{:}\, m)$ $[I_{bm}^-, \hat{x}_{bm}^-] = Info\_filter(\hat{x}_k^-, I_{inf}{}_k^-, Z_k,)$ **end** for $P_{fm}^+ = \left(I_{fm}^+\right)^{-1}$ $P_{bm}^- = (I_{bm}^-)^{-1}$ $P_m = \left[\left(P_{fm}^+\right)^{-1} + (P_{bm}^-)^{-1}\right]^{-1}$ $\hat{x}_m = P_m\left(I_{fm}^+ \hat{x}_{fm}^+ + I_{bm}^- \hat{x}_{bm}^-\right)$
Input to standard UKF	$\hat{x}_{k\|k-1}, P_{k\|k-1}, Z_{k\,DR}$
Output from standard UKF	$\hat{x}_k, P_k \;\; and \; \hat{x}_m, P_m \; when \; available$

B. FBS EVALUATION AND COMPARISON WITH UKF, EKF AND MHE RESULTS

The results associated with the FBS technique are shown in Table 8. The evaluation of the FBS was similar to the one conducted on the MHE with epi-splines. The

results obtained using the FBS are compared to the results obtained using the UKF, EKF and the MHE with epi-splines. It can be noted that the FBS managed to dock the AUV five times as shown on the highlighted cells. The FBS performed much better than the UKF and EKF methods.

Table 8. Docking Station Results for FBS in Comparison with UKF, EKF and MHE Methods

Runs	USBL Update rate	Initial Uncertainty	UKF	EKF	FBS	MHE	Docking Success				
	(Hz)	(m)	Docking error (m)	Docking error (m)	Docking error (m)	Docking error (m)	REMUS	UKF	EKF	FBS	MHE
1	0.401	20.80	3.93	4.65	2.79	0.46	No	No	No	No	No
2	0.299	16.00	8.52	9.22	6.00	0.58	No	No	No	No	No
3	0.319	22.40	3.26	4.51	2.17	0.46	No	No	No	No	No
4	0.428	15.80	4.20	5.40	3.04	0.18	No	No	No	No	Yes
5	0.436	13.70	4.23	4.87	3.01	0.08	No	No	No	No	Yes
6	0.252	8.20	3.38	3.84	1.69	0.31	No	No	No	No	Yes
7	0.209	2.50	5.53	6.32	4.10	4.82	No	No	No	No	No
8	0.351	0.00	3.09	4.01	0.23	0.98	No	No	No	Yes	No
9	0.255	2.60	3.24	4.41	2.15	1.22	No	No	No	No	No
10	0.343	0.00	6.79	7.20	5.73	0.43	No	No	No	No	No
11	0.429	3.70	2.48	3.38	0.33	0.07	No	No	No	Yes	Yes
12	0.346	6.80	1.53	2.76	1.08	0.44	No	No	No	No	No
13	0.344	4.60	2.22	2.96	0.76	0.79	No	No	No	No	No
14	0.307	5.80	1.96	3.35	0.30	0.28	No	No	No	Yes	Yes
15	0.373	8.10	1.37	3.20	1.33	1.73	No	No	No	No	No
16	0.285	9.10	0.23	0.28	0.46	0.50	Yes	Yes	Yes	No	No
17	0.501	7.50	0.72	0.53	0.32	0.43	No	No	No	Yes	No
18	0.346	15.10	1.27	0.07	0.20	2.70	Yes	No	Yes	Yes	No
19	0.283	20.00	0.13	0.50	0.90	1.60	Yes	Yes	No	No	No
Average	0.336	9.62	3.06	3.76	1.93	0.95					

The average docking error associated with FBS is 1.93 m which is much less than the docking error obtained using UKF and EKF methods. Meanwhile, the MHE algorithm successfully docked the vehicle as many times as the FBS algorithm did.

Figure 34 is Run 2 in Table 8. This figure depicts a very bad run with badly distributed USBL measurements. The FBS performed better than UKF and EKF on this run.

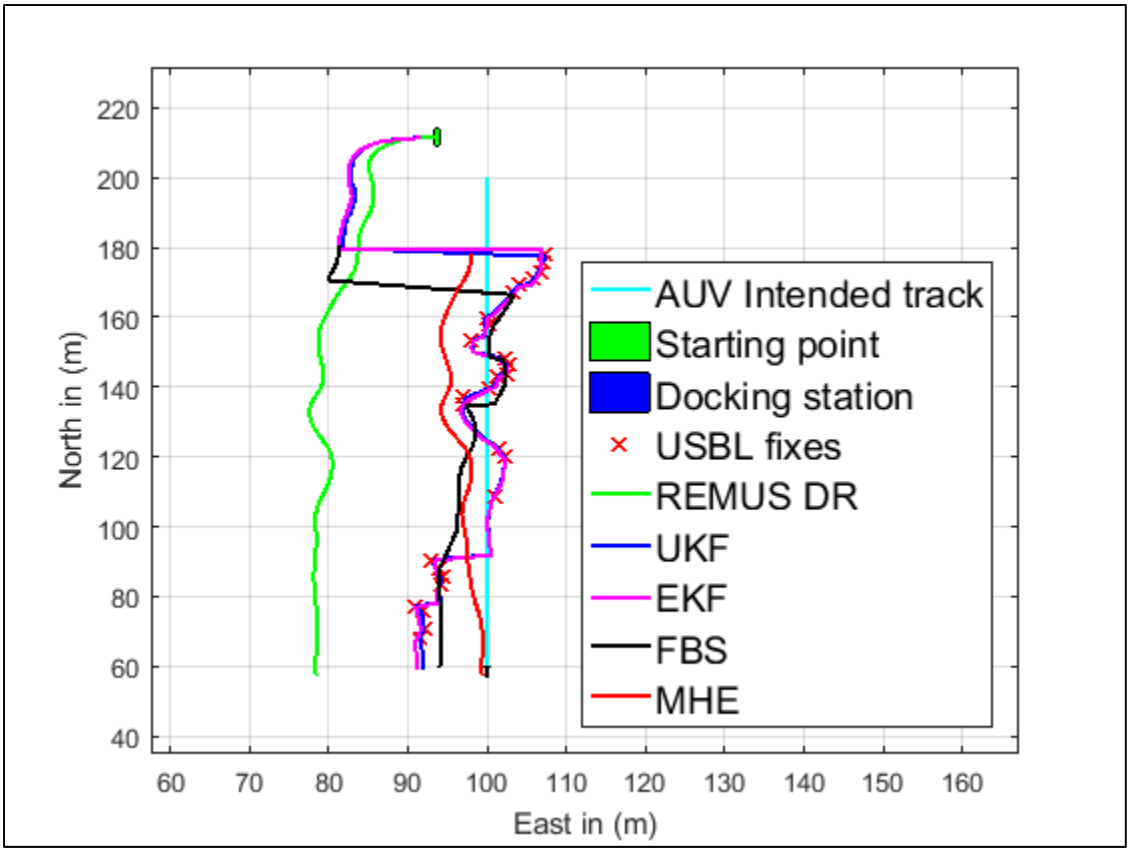

Figure 34. Run 2 with Poorly Distributed USBL Measurements

In Run 14, the FBS had a successful docking at a low USBL measurement update rate. Figure 35 illustrates the distribution of the position estimates obtained by the FBS technique and other methods analyzed during this run.

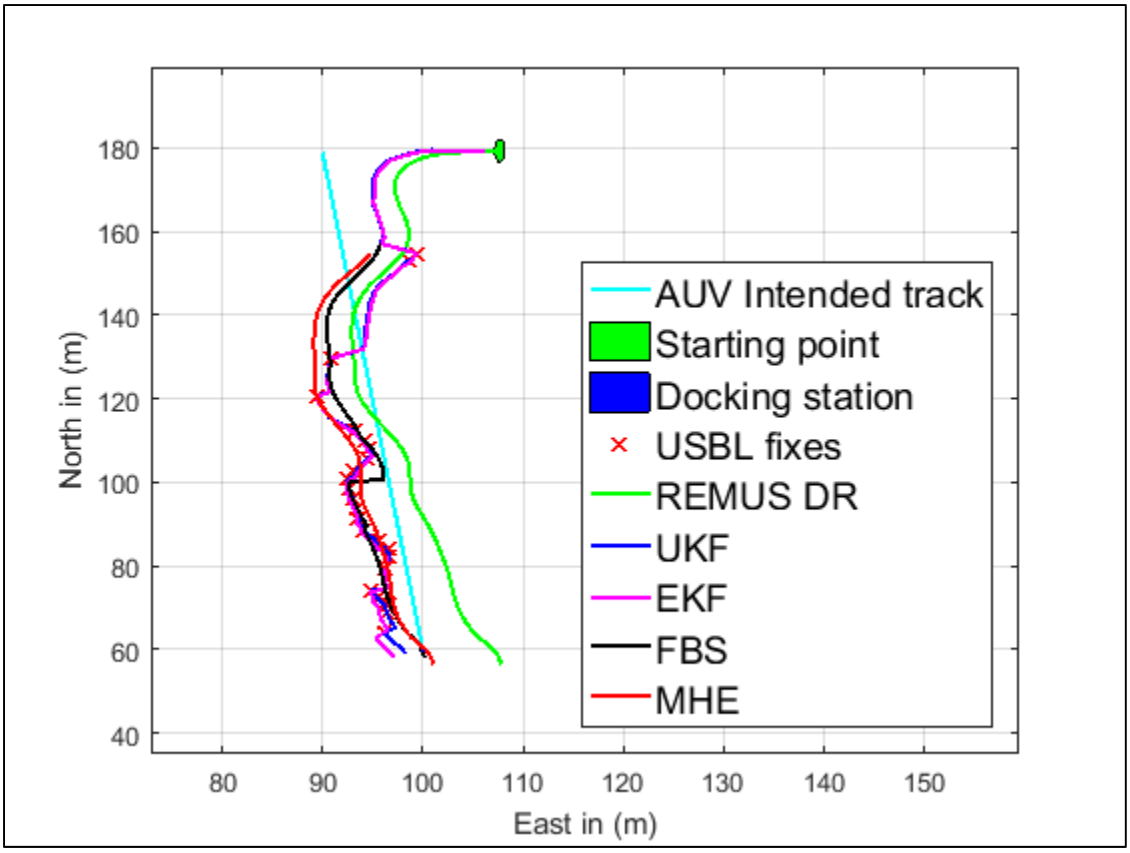

Figure 35. Run 14 with Low USBL Measurement Update Rate, FBS Docked

The FBS results demonstrate a system that does not entirely depend on the sparse, inconsistent and erroneous USBL measurements. The results indicate that FBS maintains a minimum covariance while also trying to reflect the vehicle dynamics. The strength of the FBS technique is the use of an optimal smoothed estimate to update the position of the AUV. The weakness associated with the FBS is the initialization requirement; one needs to have some knowledge of the actual position of the AUV in order to allocate the initial position for the backward smoothing process, since this method can fail to converge when initialized too far from the true initial position. Another weakness associated with the FBS is the fact that it does not use all the USBL measurements, this poses a risk of not using the best measurements.

THIS PAGE INTENTIONALLY LEFT BLANK

VII. CONCLUSION AND FUTURE WORK

A. CONCLUSION

The purpose of this study was to develop a methodology for position estimation by which sparse, erroneous, and inconsistent sensor observations can be used for autonomous underwater vehicle (AUV) terminal homing to an undersea docking station.

An undersea docking station offers great potential for increasing at-sea time and reducing survey costs of AUVs. A key part of this system is the AUV's ability to successfully dock. Part of the process for successful docking is estimating the AUV's position. The AUV's D-USBL sensor system provides range and bearing measurements to the docking station. The D-USBL range and bearing measurements are nonlinear, sparse, erroneous and inconsistent.

Position estimating methods, such as EKF and UKF were first considered and evaluated since the system is nonlinear in range and bearing measurements and these are estimation techniques for nonlinear systems. The evaluation results showed relatively poor performance for these filters.

The MHE with epi-splines was then introduced as an alternative for position estimation for the AUV to an undersea docking station. The MHE smoothing filter used the dead reckoning measurements and the D-USBL measurements as constraints for the epi-splines optimization method.

An analysis based on data sets of REMUS 100 AUV docking station runs was conducted using the MHE with epi-splines methodology and compared to EKF and UKF algorithms. The MHE with epi-splines algorithm demonstrated significantly better performance over the EKF and UKF.

A further analysis with FBS was also conducted. The FBS technique was evaluated in the same manner as the MHE with epi-splines technique, and compared with UKF, EKF and MHE with epi-splines position estimating methods. The FBS method produced better results than the UKF and EKF methods, but the MHE remained the best

method; it produced consistently better docking results on real underwater docking datasets.

The EKF had the highest average docking error of 3.76 m. The average docking error associated with UKF was 3.06 m. FBS technique had an average docking error of 1.93 m while the MHE with epi-splines had an average error of 0.95 m. It was expected that the EKF would have the highest average error due to its performance limitations when applied to systems which are highly nonlinear.

The lowest average docking error associated with the MHE indicates the great potential that the MHE has for guiding an AUV to an undersea docking station using sparse, erroneous and inconsistent USBL measurements.

B. FUTURE WORK

The opportunity to evaluate all these position estimating techniques in a real underwater docking environment was not available for this thesis. Examining the MHE with epi-splines in a real underwater docking environment could produce many successful REMUS 100 AUV dockings.

The possibilities of utilizing the UKF, EKF and FBS with a secondary in-close sensor system should be considered. The UKF, EKF and FBS results showed that they are good at tracking the USBL measurements, but these measurements (in many cases) end when the vehicle gets within 5 m of the docking station. As a result, these position estimating techniques only guide the AUV to a position about 5 m away from the docking station. A secondary in-close sensor system could provide a good solution to this problem.

Investigation on when to ignore USBL measurements should be considered for future studies. Some USBL measurements lie far from the region where most USBL measurements are concentrated. These outliers cannot realistically reflect the actual vehicle position, due to the vehicle's dynamic limitations. In this thesis, these measurements were utilized like other USBL measurements, but developing a method for eliminating spurious USBL measurements could produce better docking results.

Development of a minimal measurement characteristic (in terms of sparsity, errors and inconsistency of the USBL measurements) for successful docking should also be considered. Some sets of measurements are much more sparse, erroneous or inconsistent than other sets. Having a methodology for determining whether the USBL measurements are good or poor will assist in guiding the AUV since poor USBL measurements will be rejected.

THIS PAGE INTENTIONALLY LEFT BLANK

LIST OF REFERENCES

[1] D. Horner and M. Mqana, "Moving horizon estimate for undersea docking," unpublished.

[2] What We Do. (n.d.). REMUS. [Online]. Available: http://www.whoi.edu/main/remus, Accessed Jan 07, 2017.

[3] *REMUS Operations & Maintenance Manual*, Kongsberg, Norway: Kongsberg Maritime, 2007.

[4] B. W. Hobson et al., "Development and ocean testing of an AUV docking station for a 21" AUV," in *Oceans*, Vancouver, BC, 2008, pp. 1–6.

[5] C. J. von Alt et al., "A well sampled ocean," *Oceanus Magazine*, vol. 42, no. 1, pp. 1–3, Jan. 2000.

[6] M. D. Feezer et al., "Autonomous underwater vehicle homing/docking via electromagnetic guidance," *IEEE J. Ocean. Eng.*, vol. 26, no. 4, pp. 515–521, Oct. 2001.

[7] G. Baratoff and S. Blansteen. (n.d.). Tracking devices, [Online]. Available: http://www.hitl.washington.edu/research/knowledge_base/virtual-worlds/EVE/I.D.1.b.TrackingDevices.html

[8] A. Myagotin et al., "AUV positioning model employing acoustic and visual data processing," *IEEE Oceans 2010-Sydney*, pp. 1–7, Oct 2010.

[9] F. Mandić et al., "Underwater object tracking using sonar and USBL measurements," *J. Sensors*, vol. 2016, pp. 1–10, Jul. 2016.

[10] N. Stilinović et al., "Guidance and control of an overactuated autonomous surface platform for diver tracking," in *21st Mediterranean Conf. Control & Automation (MED)*, 2013, pp. 1–6.

[11] Ø. Hegrenaes et al., "Underwater transponder positioning and navigation of autonomous underwater vehicles," in *Oceans*, Biloxi, MS, 2009, pp. 1–7.

[12] P. J. Frontera, "Nonlinear estimation with sparse temporal measurements," Ph.D. dissertation, Dept. Mech. Aero. Eng., Naval Postgraduate School, Monterey, CA, 2016. [Online]. Available: http://hdl.handle.net/10945/50547

[13] Y. O. Mohammed and A. J. Alzubaidi, "Missile position tracking using Kalman filter," *IOSR J. Eng.*, vol. 4, no. 2, pp. 43–45, Feb. 2014.

[14] M. S. Bezick et al., "Inertial navigation for guided missile systems," *Johns Hopkins APL Tech. Dig.*, vol. 28, no. 4, pp. 331–342, Nov. 2010.

[15] N. Nadarajah et al., "Multitarget tracking using probability hypothesis density smoothing," *IEEE Trans. Aerosp. Electron. Syst.*, vol. 47, no. 4, pp. 2344–2360, Oct. 2011.

[16] S. Kim et al., "Kalman filtering for relative spacecraft attitude and position estimation," *AIAA J. Guidance, Control, and Dynamics*, vol. 30, no.1, pp. 133–143, Jan.–Feb. 2007.

[17] J. O. Royset and R. J. B. Wets. (2014). From data to assessments and decisions: epi-spline technology. Dept. Operations Res., Naval Postgraduate School. Monterey, CA. [Online]. Available: http://hdl.handle.net/10945/50547

[18] M. W. Mehrez et al., "Nonlinear moving horizon state estimation for multi-robot relative localization," in *IEEE 27th Canadian Conf. Elect. Comput. Eng.* Toronto, Canada, 2014, pp. 1–5.

[19] L. Andong and Z. Wen-An, "Moving horizon estimation for mobile robots with multirate sampling," *IEEE Trans. Ind. Electron.*, vol. 64, no. 2, pp. 1457–1467, Feb. 2017.

[20] M. K. Ramalingam, "Moving horizon estimation with dynamic programming," M.S. thesis, Dept. Chemical Biomedical Eng., Cleveland State Univ., OH, 2013.

[21] M. A. Müller, "Nonlinear moving horizon estimation for systems with bounded disturbances," *Automatica*, vol. 79, pp. 306–314, May 2017.

[22] M. Zanon et al., "Nonlinear moving horizon estimation for combined state and friction coefficient estimation in autonomous driving," in *European Control Conference*, Zurich, SUI, pp. 1–6, 2013.

[23] D. J. Simon, *Optimal State Estimation*, New Jersey, John Wiley & Sons, 2006, pp. 18–285.

[24] E. B. Bermudez, "Terminal homing for autonomous underwater vehicle docking," M.S. thesis, Dept. Mech. Aero. Eng., Naval Postgraduate School, Monterey, CA, 2016.

[25] T. I. Fossen, *Guidance and Control of Ocean Vehicles*. New York: John Wiley and Sons, 1994.

[26] E. A. Wan and R. van der Merve, "The Unscented Kalman filter for nonlinear estimation," Oregon Graduate Inst. Sci. & Technol.

[27] Stochastic error identification and modelling. (n.d.). Institute of Flight System Dynamics. [Online]. Available: http://www.fsd.mw.tum.de/research/sensors-data-fusion-and-navigation/research-and-competence-areas/data-fusion/. Accessed May 20, 2017.

[28] M. Rhudy and Y. Gu, "Understanding nonlinear Kalman filters, part II: An implementation guide," *Interactive Robotics Letters*, West Virginia University, Jun. 2013.

[29] G. A. Einicke, and L. B. White, "Robust extended Kalman filtering," *IEEE Trans. Signal Process.*, vol. 47, no. 9, pp. 2596–2599, Sep. 1999.

[30] S. J. Julier and J. K. Uhlmann, "A new extension of the Kalman filter to nonlinear systems," Dept. Eng. Sci., Robotics Research Group, University of Oxford, UK.

[31] J. O. Royset and R. J. B. Wets. (2015). "Nonparametric Density Estimation via Exponential Epi-Splines: Fusion of Soft and Hard Information," *European Journal of Operational Research,* vol. 247, no. 2, pp. 532–547, 2015.

[32] E. L. Haseltime and J. B. Rawlings, "A critical evaluation of extended Kalman filtering and moving horizon estimation," in *Texas-Wisconsin Modeling and Control Consortium*, 2003, pp. 1–48.

[33] J. O. Royset and R. J. B. Wets. (2016). "Mutivariate epi-splines and evolving function identification problems," Set-Valued and Variational Analysis, vol. 24, no. 4, pp. 517–545, 2016.

[34] P. M. P. Tydingco, "The use of epi-splines to model empirical semivariograms for optimal spatial estimation," M.S. thesis, Dept. Operations Res., Naval Postgraduate School, Monterey, CA, 2016.

THIS PAGE INTENTIONALLY LEFT BLANK

INITIAL DISTRIBUTION LIST

1. Defense Technical Information Center
   Ft. Belvoir, Virginia

2. Dudley Knox Library
   Naval Postgraduate School
   Monterey, California